HHS Public Access

Author manuscript

J Control Release. Author manuscript; available in PMC 2023 October 01.

Published in final edited form as:

J Control Release. 2022 October ; 350: 584–599. doi:10.1016/j.jconrel.2022.08.045.

Simultaneous crosslinking of CD20 and CD38 receptors by drug-free macromolecular therapeutics enhances B cell apoptosis in vitro and in vivo

M. Tommy Gambles[a,b], **Jiahui Li**[a,b], **D. Christopher Radford**[a,d], **Douglas Sborov**[c], **Paul Shami**[c], **Jiyuan Yang**[a,b,**], **Jindřich Kopeček**[a,b,d,*]

[a]Center for Controlled Chemical Delivery, University of Utah, Salt Lake City, UT 84112, USA

[b]Department of Pharmaceutics and Pharmaceutical Chemistry, University of Utah, Salt Lake City, UT 84112, USA

[c]Huntsman Cancer Institute, University of Utah, Salt Lake City, UT 84112, USA

[d]Department of Biomedical Engineering, University of Utah, Salt Lake City, UT 84112, USA

Abstract

Drug-Free Macromolecular Therapeutics (DFMT) is a new paradigm in macromolecular therapeutics that induces apoptosis in target cells by crosslinking receptors without the need of low molecular weight drugs. Programmed cell death is initiated via a biomimetic receptor crosslinking strategy using a two-step approach: i) recognition of cell surface antigen by a morpholino oligonucleotide-modified antibody Fab' fragment (Fab'-MORF1), ii) followed by crosslinking with a multivalent effector motif – human serum albumin (HSA) grafted with multiple complementary morpholino oligonucleotides (HSA-$(MORF2)_x$). This approach is effective in vitro, in vivo, and ex vivo on cells from patients diagnosed with various B cell malignancies. We have previously demonstrated DFMT can be applied to crosslink CD20 and CD38 receptors to successfully initiate apoptosis. Herein, we show simultaneous engagement, and subsequent crosslinking of both targets ("heteroreceptor crosslinking"), can further enhance the apoptosis induction capacity of this system. To accomplish this, we incubated Raji (CD20+; CD38+) cells simultaneously with anti-CD20 and anti-CD38 Fab'-MORF1 conjugates, followed by addition of the macromolecular crosslinker, HSA-$(MORF2)_x$ to co-cluster the bound receptors.

*Correspondence to: J. Kopeček, University of Utah, Center for Controlled Chemical Delivery, 2030 East 20 South, Biopolymers Research Building, Room 205B, Salt Lake City, UT 84112-9452, USA. jindrich.kopecek@utah.edu (J. Kopeček). **Correspondence to: J. Yang, University of Utah, Center for Controlled Chemical Delivery, 2030 East 20 South, Biopolymers Research Building, Room 205C, Salt Lake City, UT 84112-9452, USA. jiyuan.yang@utah.edu (J. Yang).

CRediT authorship contribution statement

M. Tommy Gambles: Conceptualization, Methodology, Investigation, Data curation, Writing - review & editing. **Jiahui Li:** Methodology, Investigation. **D. Christopher Radford:** Methodology. **Douglas Sborov:** Validation, Funding acquisition. **Paul Shami:** Validation. **Jiyuan Yang:** Conceptualization, Funding acquisition, Supervision. **Jindřich Kopeček:** Conceptualization, Methodology, Validation, Funding acquisition, Supervision, Writing - review & editing.

Declaration of Competing Interest

The authors declare the following competing financial interest(s): J. Y. and J.K. are co-inventors on a pending US patent application (PCT/US2014/023784; assigned to the University of Utah) related to this work. J.K. is Chief Scientific Advisor and J.Y. Scientific Advisor, and P.S. Chief Medical Advisor for Bastion Biologics. Otherwise, the authors declare no competing financial interests.

Appendix A. Supplementary data

Supplementary data to this article can be found online at https://doi.org/10.1016/j.jconrel.2022.08.045.

Fab' fragments from Rituximab and Obinutuzumab were employed in the synthesis of anti-CD20 bispecific engagers (Fab'$_{RTX}$-MORF1 and Fab'$_{OBN}$-MORF1), whereas Fab' fragments from Daratumumab and Isatuximab (Fab'$_{DARA}$-MORF1 and Fab'$_{ISA}$-MORF1) targeted CD38. All heteroreceptor crosslinking DFMT combinations demonstrated potent apoptosis induction and exhibited synergistic effects as determined by Chou-Talalay combination index studies (CI < 1). In vitro fluorescence resonance energy transfer (FRET) experiments confirmed the co-clustering of the two receptors on the cell surface in response to the combination treatment. The source of this synergistic therapeutic effect was further explored by evaluating the effect of combination DFMT on key apoptosis signaling events such as mitochondrial depolarization, caspase activation, lysosomal enlargement, and homotypic cell adhesion. Finally, a xenograft mouse model of CD20+/CD38+ Non Hodgkin lymphoma was employed to demonstrate in vivo the enhanced efficacy of the heteroreceptor-crosslinking DFMT design versus single-target systems.

Keywords

CD20 and CD38; Drug-free macromolecular therapeutics; Morpholino oligonucleotides; Human serum albumin; Lymphoma; Multiple myeloma

1. Introduction

Hematopoietic malignancies make up a significant margin of total cancer diagnoses [1]. In 2020, 10 % of all new cancer diagnoses were hematopoietic malignancies. Current therapy options for these malignancies include resection, chemotherapy, radiotherapy, targeted gene therapy, immunotherapy, bone marrow transplant (hematopoietic stem cell transplant), or a combination of any or all of these therapies [2,3]. Although many treatment options are available, no definitive cure is available for patients with specific subtypes of leukemia and lymphoma or multiple myeloma (MM) [4]. In many B cell malignancies, immunotherapy with a monoclonal antibody (mAb) is combined with chemotherapy or other novel therapeutics [5,6]. For example, the most common combinational treatment for non-Hodgkin lymphoma patients includes the combination of anti-CD20 mAb, rituximab, with *"CHOP"* (cyclophosphamide, doxorubicin, Oncovin (vincristine), and prednisone (corticosteroid)) – a combination of chemotherapy and immunosuppressant reagents [7]. The shortcoming of current therapies is the persistence of malignant cells that show resistance to the therapies used [8,9]. Multidrug resistant leukocytic malignancies, including rituximab-resistant variants, are well characterized and occur in the majority of relapsed hematologic malignancies [10,11].

The administration of mAbs targeting over-expressed antigens on hematopoietic cancer cell surfaces leads to cell death via several potential mechanisms: antibody-dependent cellular cytotoxicity (ADCC), complement-dependent cytotoxicity (CDC), antibody-dependent cellular phagocytosis (ADCP), and direct apoptosis upon receptor crosslinking [12,13]. Immunotherapy induces selective pressures toward low expressing antigen cell populations that can evade these mechanisms leading to change in cancer phenotype and therapy-resistance [14]. Better and/or more potent therapies are needed to overcome the problem of resistance.

Drug Free Macromolecular Therapeutics (DFMT) is a biomimetic antigen-receptor crosslinking technology our group has developed previously [15-19]. We have demonstrated the system's ability to induce apoptosis upon crosslinking of CD20 or CD38 receptors on the surface of malignant B cells [20,21]. DFMT is comprised of a two-step therapeutic approach that features sequential treatment of a modified monoclonal antibody Fab' targeting motif followed by a multivalent effector – crosslink-inducing macromolecule – to induce apoptosis in the target cell without the use of small molecule chemotherapeutics. Biorecognition between the modified Fab' fragment targeting motif and the crosslink-inducing macromolecule is accomplished through hybridization of complementary morpholino oligonucleotide strands. The Fab' fragment is modified with a single morpholino oligomer (MORF1); and human serum albumin (HSA) is modified with multiple complementary morpholino oligomers (MORF2). DFMT works via a pre-targeting approach of the modified Fab'-MORF1 molecule followed by, in a time-dependent manner, the crosslink-inducing macromolecule HSA-$(MORF2)_{10}$. The Fab'-MORF1 nanoconjugates can be used as pre-targeting agents that exhibit no direct efficacy on their own; however, induce a therapeutic effect upon crosslinking via hybridization with the multivalent HSA-$(MORF2)_{10}$ delivered as the active dose. A 5 h time lag in vivo between administration of the two nanoconjugates [16] allows for: i) low steady state plasma concentration of Fab'-MORF1 due to clearance of unbound Fab'-MORF1 from the blood; and ii) off-target Fab'-MORF1 binding will be internalized and degraded. Anti-CD20 and anti-CD38 DFMT systems have been developed and demonstrate the effectiveness of this system on antigen expressing cells [20-22]. DFMT has been shown to induce apoptosis in numerous cell lines in vitro, has proven efficacious against cells isolated from patients diagnosed with various B cell malignancies [23], and has shown efficacy in reducing cancer load and increasing life expectancy in xenograft Non-Hodgkin Lymphoma (NHL) mouse models [16,20,24].

The concept of heterocrosslinking of dual receptors mediated by nanocarriers has been considered previously [25,26]. Heteroreceptor targeting has also been pursued by the advent of immunotherapeutic systems including T-cell redirecting bispecific antibodies (bsAbs) and tandem bodies [27,28]. Bispecific antibodies validated the concept and demonstrated that targeting two different antigens serves to alleviate some of the shortcomings of standard monoclonal antibodies. The capacity to target two different antigens simultaneously could mitigate occurrence of mAb resistance and has the potential to induce better targeting and increased ADCC and CDC killing of target cells [29].

It is well established that two different mAbs may induce apoptosis through different mechanisms. For example, two anti-CD20 antibodies, rituximab (RTX) and obinutuzumab (OBN), target the same receptor antigen, but have distinct binding epitopes that elicit cellular response via different mechanisms of action [30]. Type I antibodies induce apoptosis via calcium influx, mitochondrial depolarization, and caspase activation while Type II antibodies induce apoptosis via actin destabilization, lysosomal breakage, and homotypic cell adhesion. RTX (Type I) induces apoptosis through the traditional routes of receptor crosslinking, ADCC and CDC; however, OBN (Type II) was designed to induce apoptosis directly upon CD20 receptor engagement, without the need for crosslinking. We have previously reported a Type II antibody like OBN can be given additional Type I antibody characteristics by crosslinking with DFMT [24]. Furthermore, different cell surface

receptors provide different functions for the cell. CD20 is involved in calcium channeling and proper B cell immune response [3,31,32]. CD38 is also involved in calcium influx and signal transduction [33] but has enzymatic function where it hydrolyzes cyclic ADP ribose [34]. It is thought that anti-CD38 mAbs, daratumumab (DARA) and isatuximab (ISA), inhibit this enzymatic function as part of their mechanism of action [35]. Dual-targeting DFMT may increase efficacy because of the inhibition of two cellular functions of two different receptors simultaneously. Potentially, synergistic drug combination effects might be observable and methods to delineate synergistic effects from additive effects are known. The Chou-Talalay method provides a mathematical approach to distinguish synergism from additive effects when combining two therapeutics [36]. A “combination index” (CI) is calculated from data points in combination experiments – where CI values < 1 indicate synergism, CI values roughly equal to one indicate additive effects, and CI values > 1 indicate antagonistic effects.

Here, we report the simultaneous crosslinking of CD20 and CD38 receptors using a dual-targeting DFMT approach that significantly increases apoptosis induction in CD20+/CD38+ NHL cells (Raji). We show simultaneous crosslinking of multiple target antigens with Fab’-MORF1 cocktails, followed by HSA-$(MORF2)_{10}$ crosslinking, enhances apoptotic effects of DFMT over individual receptor crosslinking. To this end, we evaluated the impact of coinciding heteroreceptor crosslinking of CD20 receptors with CD38 receptors. We synthesized Fab’-MORF1 DFMT nanoconjugates for two anti-CD20 mAbs (Fab'_{RTX}-MORF1 and Fab'_{OBN}-MORF1) and two anti-CD38 mAbs (Fab'_{DARA}-MORF1 and Fab_{ISA}-MORF1). We evaluated each single-target Fab’ DFMT system compared to combination Fab’ DFMT systems comprised of one anti-CD20 Fab’-MORF1 and one anti-CD38 Fab’-MORF1. Combination DFMT was assessed in terms of apoptosis-induction, degree of synergism, cellular apoptotic mechanisms of action, and in vivo evaluation of Fab'_{RTX} + Fab'_{DARA} DFMT combination therapy using a NHL mouse model.

2. Materials and methods

2.1. Materials

The 25-base pair phosphorodiamidate morpholino oligonucleotides, MORF1 and MORF2, were customized and purchased from Gene Tools (Philomath, OR, USA). Specific modifications for the two complementary strands included a 3′ primary amine on MORF1 (5′-GAGTAAGCCAAGGAGAATCAATATA-NH_2–3′) and a 3′ disulfide handle on MORF2 (5′TATATTGATTCTCCTTGGCTTACTC-S-SR-3′). Human serum albumin (chromatographically and fractionation purified with purity >95%) was purchased from Innovative Research (Peary Court Novi, MI, USA). Daratumumab (Darzalex®, Janssen Biotech (Harsham, PA, USA), Isatuximab (Sarclisa®), Obinutuzumab (Gazyva®), and Rituximab (Rituxan®) were acquired from Huntsman Cancer Hospital, University of Utah. Tris(2-carboxyethyl) phosphine (TCEP) and the heterobifunctional $SM(PEG)_2$ linker (succinimidyl-([*N*-maleidopropionamido]-diethyleneglycol) ester) were purchased from Thermo Fisher Scientific (Rockford, IL, USA). Pepsin (porcine gastric mucosa) was purchased from Sigma-Aldrich (St. Louis, MO, USA). Cy3- and Cy5-NHS (*N*-hydroxysuccinimide ester) were purchased from Lumiprobe (Hallandale Beach, FL,

USA). Fluo-3 AM (4-(6-acetoxymethoxy-2,7-dichloro-3-oxo-9-xanthenyl)-4′-methyl-2,2′ (ethylenedioxy)dianiline-*N,N,N′,N′*-tetra-acetic acid tetrakis(acetoxymethyl) ester), JC-1 (5,5′,6,6′-tetrachloro-1,1′,3,3′-tetraethylbenzimidazoylcarbocyanine iodide), and CCCP (carbonyl cyanide 3-chlorophenylhydrazone) were purchased from Invitrogen (Carlsbad, CA, USA). Anti-Bcl-2 (100) Alexa Fluor® 488 mAb and anti-Bax (2D2) Alexa Fluor® 647 mAb were purchased from Santa Cruz Biotechnology (Dallas, TX, USA). *APC*-anti-human CD19 (mouse IgG1, κ isotype) and *PE*-anti-human CD10 (mouse IgG1, κ isotype) were purchase from BioLegend. PhiPhiLux® kit was purchased from OncoImmunin (Gaithersburg, MD, USA). Lysosome tracker Green DND-26, H_2DCFDA (2′,7′-dichlorofluorescein), Cytochrome C ELISA kit (human) and Cholera Toxin Subunit B Alexa Fluor® 555 were purchased from Thermo Fisher. All solvents were purchased from Fisher Scientific at the highest purity available.

2.2. Animals

Female SCID C·B-17 mice with double B and T cell knockouts through *Prkdc*$^{-/-}$ mutation were purchased from Charles River Laboratories (Wilmington, MA). All experiments involving animals were performed according to the protocol approved by the Institutional Animal Care and Use Committee (IACUC) of the University of Utah.

2.3. Synthesis and characterization of nanoconjugates

2.3.1. Fab′-MORF1 Nanoconjugates—Four Fab′-MORF1 (two anti-CD20 and two anti-CD38) nanoconjugates were synthesized as previously described [37]. Briefly, monoclonal antibody is digested with pepsin followed by reduction using TCEP to generate the freshly reduced Fab' species with sulfhydryl groups (Fab'-SH). Fab'-SH is immediately conjugated with maleimide functionalized MORF1 via thiol-maleimide *click* chemistry to yield the desired Fab'-MORF1 nanoconjugate. An example synthesis is as follows: Rituxan® was buffer exchanged into citrate buffer pH 4.0 to yield pure Rituximab mAb in buffer. Pepsin (10 *w/w%*) was added to the RTX solution and the digestion was continued at 37 °C until completion (reaction was monitored with size exclusion chromatography (SEC) on AKTApure to determine complete digestion by observing disappearance of RTX whole antibody peak and emergence of the F(ab')$_2$ peak; roughly 90 min). F(ab')$_2$ was purified using centrifugal ultrafiltration (30,000 MWCO membrane, several 5× volume PBS washes; purity assessed with SEC). Fab'-SH was produced and used fresh for each reaction by reducing F(ab')$_2$ (4 mg, 4 mg/mL) with TCEP (4.6 mg, 20 mM) in 100 mM citric acid buffer pH 5.5 for 2 h at 37 °C. Fab'-SH was purified using centrifugal ultrafiltration (10,000 MWCO membrane, several 5× volume PBS washes). Reaction completion and purity were assessed with SEC. MORF1-PEG$_2$-Mal was synthesized in parallel by conjugating SM (PEG)$_2$ (4.25 mg, 10 μmol) dissolved in 50 μL DMSO with MORF1 (1.8 mg, 200 nmol) dissolved in 150 μL PBS 7.4 buffer. Reaction was continued for 2 h at room temperature. The desired MORF1-PEG$_2$-Mal product was purified using centrifugal ultrafiltration (3000 MWCO membrane, several 5× volume PBS washes). Pure MORF1-PEG$_2$-Mal (1.2 equiv.) was conjugated with fresh Fab'-SH (1 equiv.) by thiol-maleimide *click* chemistry reaction for 3 h at room temperature in PBS pH 6.5 buffer. The final product was purified by centrifugal ultrafiltration (30,000 MWCO membrane, 8× volume washes) with PBS pH 7.4 buffer. Fab' concentration was determined by BCA analysis and MORF1 concentration

was determined using NanoDrop ND-1000 spectrophotometer at 260 nm (ε = 278,000 M^{-1} cm^{-1} in 0.1 N HCl_{aq}). Fab'$_{RTX}$-MORF1, Fab'$_{DARA}$-MORF1, Fab'$_{ISA}$-MORF1, and Fab'$_{OBN}$-MORF1 nanoconjugates were each synthesized following this protocol.

2.3.2. HSA-(MORF2)$_{10}$ crosslink-inducing macromolecule—HSA-(MORF2)$_{10}$ was synthesized in two steps as previously reported [22]. First, lysine primary amine groups at the periphery of the HSA molecule were decorated with SM(PEG)$_2$ via nucleophilic substitution of the NHS ester groups on SM(PEG)$_2$-The resulting product was an HSA molecule with multivalent maleimide functional groups on its periphery (HSA-(PEG$_2$-Mal)$_y$). In parallel, MORF2-disulfide was reduced with TCEP, purified and immediately reacted with HSA-(PEG$_2$-Mal)$_y$ to yield the desired multivalent product HSA-(MORF2)$_x$. Briefly, HSA (5 mg, 3.9 μmol NH_2 equiv.) was dissolved in 400 μL PBS pH 7.4 buffer. SM(PEG)$_2$ (18.3 mg, 10 eq.) in 150 μL DMSO was added to the HSA solution. The reaction was stirred for 2 h at room temperature to yield HSA-(PEG$_2$-Mal)$_y$. The product was purified using centrifugal ultrafiltration (30,000 MWCO, 5× volume washes). The number of maleimide groups per HSA was determined by a modified Ellman's assay, coupled with BCA protein concentration assay. In parallel, MORF2-disulfide (2.89 mg) was reduced with TCEP (10 mM) in 250 μL PBS pH 7.4 at 37 °C for 45 min to yield MORF2-SH. MORF2-SH was purified by centrifugal ultrafiltration (3000 MWCO, 5× volume wash). Freshly reduced MORF2-SH (2 equiv.) and freshly maleimide-functionalized HSA-(PEG$_2$-Mal)$_y$ (1 equiv. of maleimide) were conjugated via thiol-maleimide *click* chemistry for 3 h at room temperature in PBS pH 6.5 buffer to yield the desired product HSA-(MORF2)$_{10}$. HSA-(MORF2)$_{10}$ was purified by centrifugal ultrafiltration (30,000 MWCO membrane, 8× volume washes) and purity confirmed by SEC using AKTApure. The substitution number of MORF2 per HSA molecule was determined by a combination of BCA assay and UV spectrophotometry (260 nm, ε = 252,000 M^{-1} cm^{-1} in 0.1 N HCl_{aq}).

2.3.3. MORF1-MORF2 nanoconjugate hybridization—Fab′-MORF1 hybridization with HSA-(MORF2)$_{10}$ in solution was validated by mixing the two complementary MORF conjugates in solution and observing changes in optical density at 260 nm (ND-1000 spectrophotometer) that is a reflection of the hypochromic effect. Particularly, Fab'$_{RTX}$-MORF1 was added to a solution of HSA-(MORF2)$_{10}$ at varying ratios in PBS 7.4 buffer. After 10 min, the optical density at 260 nm was recorded. Additionally, MORF1-MORF2 hybridization between conjugates was confirmed by SEC by comparison of pure nanoconjugates spectra with the hybridized mixtures.

2.4. Cell culture

Human Burkitt's B-cell Non-Hodgkin Lymphoma Raji cells were purchased from the American Type Culture Collection (ATCC). Raji cells were cultured in RPMI-1640 medium supplemented with 10% fetal bovine serum (FBS), penicillin (100 units mL^{-1}) and streptomycin (0.1 mg/mL) at 37 °C in 5% CO_2 humidified atmosphere.

2.5. Apoptosis assay

In vitro apoptosis analysis of DFMT-treated cells was quantified using Annexin V / Propidium Iodide staining and analyzed by flow cytometry. The apoptotic response of

$CD20^+/CD38^+$ Raji cells treated with CD20-targeting DFMT, CD38-targeting DFMT, or combinational DFMT were evaluated. In each case, the ratio of MORF1:MORF2 was maintained at 1:1. Therefore, combination DFMT treatment groups that incorporated the use of two different Fab'-MORF1 nanoconjugates administered together, used half the concentration of each Fab'-MORF1. Specifically, 2×10^5 cells were loaded into the wells of a 24-well plate with a total volume of 400 μL medium per well. Cells were first incubated with Fab'-MORF1 for 1 h, followed by PBS wash and resuspension in fresh medium. Cells were then incubated for 24 h with HSA-$(MORF2)_{10}$ and analyzed for apoptosis by Annexin V / Propidium Iodide staining. Untreated cells were used to gate Annexin V / Propidium Iodide −/− population. Each treated cohort was then compared to untreated. DFMT efficacy values are reported as the percentage of Annexin V positive cells. All treatments were performed in triplicate and repeated for several replicates for each DFMT combination system.

Combination experiments included:

Fab'_{ISA}-MORF1 (25 μM) + Fab'_{RTX}-MORF1 (25 μM) / HSA-$(MORF2)_{10}$ (50 μM)

Fab'_{ISA}-MORF1 (25 μM) + Fab'_{OBN}-MORF1 (25 μM) / HSA-$(MORF2)_{10}$ (50 μM)

Fab'_{DARA}-MORF1 (25 μM) + Fab'_{RTX}-MORF1 (25 μM) / HSA-$(MORF2)_{10}$ (50 μM)

Fab'_{DARA}-MORF1 (25 μM) + Fab'_{OBN}-MORF1 (25 μM) / HSA-$(MORF2)_{10}$ (50 μM)

Each combination apoptosis efficacy experiment was controlled by performing single-target DFMT therapy at both 25 μM and 50 μM.

2.6. DFMT titration EC_{50} experiments

Raji cells (2×10^5) were added to the wells of a 24-well plate in 400 μL RPMI-1640 medium. Serial dilutions of each nanoconjugate solution were prepared and cells were treated with the titrated nanoconjugate solutions at concentrations of [MORF1] = [MORF2] = 1 μM, 100 nM, 10 nM, 1 nM, 100 μM, and 10 μM. Standard DFMT protocol of 1 h Fab'-MORF1, followed by PBS wash, followed by 24 h of HSA-$(MORF2)_{10}$ incubation was followed. After 24 h, cells were collected, washed with PBS, stained with Annexin V / Propidium Iodide and percent apoptotic cells determined by flow cytometry. Percent apoptotic cells were normalized to maximum apoptosis and are overlayed with fluorescently labeled Fab'-MORF1 binding data. Each treatment group was performed in triplicate and experiments were replicated two times.

2.7. Cy5/Cy3- Fab'-MORF1 binding

Raji cells (2×10^5) were incubated with serial dilution concentrations of fluorescently labeled Fab'-MORF1 nanoconjugates for 1 h at 4 °C. Then, cells were collected, washed with PBS, and analyzed by flow cytometry for fluorescence. Fluorescence intensity at each concentration were normalized to maximum fluorescence and graphed against normalized apoptosis. Each treatment group was performed in triplicate and experiments were replicated two times.

2.8. Determination of Chou-Talalay combination index

The EC_{50} values for each single-target DFMT were obtained from the DFMT titration experiments. Using the known EC_{50} values, combination experiments were designed by treating Raji cells (2×10^5 cells/well, 24-well plate, 400 μL total volume) with two different Fab'-MORF1 nanoconjugates simultaneously at various multiples of their respective EC_{50} values. One anti-CD20 Fab'-MORF1 (Fab'$_{RTX}$-MORF1 or Fab'$_{OBN}$-MORF1) was combined with one anti-CD38 Fab'-MORF1 (Fab'$_{DARA}$-MORF1 or Fab'$_{ISA}$-MORF1), for a total of four possible combinations. Cells were incubated with Fab'-MORF1 cocktails of serial diluted concentrations based on the respective EC_{50}. The highest concentration was 4× the EC_{50} and diluted by halves down to 1/8× the EC_{50} (see Figs. S5 - S9 for detailed information regarding treatment conditions). Cells were incubated with the Fab'-MORF1 combinations for 1 h, followed by PBS wash, and treatment with HSA-$(MORF2)_{10}$ for 24 h. After 24 h, cells were collected, washed with PBS, stained with Annexin V / Propidium Iodide, and analyzed for apoptosis with flow cytometry. Experiments were performed in triplicate and replicated two times for each combination.

Total apoptotic cells per treatment group were tabulated and converted to fraction of affect cells (F_a) by normalizing each experiment to maximum apoptosis. The F_a value was then used to calculate and plot various drug combination parameters including Median-Effect Plots, Dose-Effect Curves, Isobolograms and Combination Index Plots. The combination index values for each DFMT combination are reported at effective doses of 75%, 90% and 95% of affected cells.

2.9. CD20 / CD38 co-clustering FRET experiments

Two labeled Fab'-MORF1 nanoconjugates for FRET studies were synthesized as described above with modifications. Cy3-NHS and Cy5-NHS fluorophores were conjugated to freshly reduced Fab'-SH immediately before conjugation with MORF1-PEG_2-Mal. Cy3-Fab'$_{RTX}$-MORF1 and Cy5-Fab'$_{DARA}$-MORF1 were the two nanoconjugates used for FRET analysis. Cells were incubated with both Fab'-MORF1s (500 nM each Fab'-MORF1) simultaneously for 1 h at 4 °C. Receptor-bound Fab'-MORF1s were then either crosslinked by the addition of the crosslink-inducing HSA-$(MORF2)_{10}$ or were left "un-crosslinked". Cells were analyzed using flow cytometry and confocal microscopy for FRET emission. FRET emission was quantified as the amount of fluorescence observed when exciting cells with a 488 nm excitation with 530 / 30 nm band-pass filter and detecting emission 670 / 30 nm. Cy3 "bleed-through" into the FRET channel was controlled for by treating cells with Cy3-Fab'$_{RTX}$-MORF1 and unlabeled Fab'$_{DARA}$-MORF1. Cy5 "bleed- through" was controlled for by treating cells with unlabeled Fab'$_{RTX}$-MORF1 and Cy5-Fab'$_{DARA}$-MORF1. In summary, FRET signal from crosslinked Fab'-MORF1's was compared to un-crosslinked Fab'-MORF1s. As receptor-bound Fab'-MORF1 conjugates were forced closer together via crosslinking, FRET signal should increase if crosslinking of CD20 with CD38 occurs.

2.10. Calcium influx by flow cytometry

Raji cells (2×10^5) were loaded with Fluo-3 AM calcium indicator (5 μM) in 400 μL RPMI-1640 media for 30 min at 37 °C. Cells were washed and resuspended in RPMI-1640 media supplemented with 2.5 mM Ca^{2+} and were treated with various combinations of

DFMT therapies, either single target or heteroreceptor DFMT for 1 h. After 1 h, cells were washed with PBS and taken for flow cytometry analysis to quantify fluorescence of Fluo-3 AM in the treated cells.

2.11. Calcium influx by confocal microscopy

Raji cells (2×10^5) were loaded with Fluo-3 AM calcium indicator (5 μM) in 400 μL RPMI-1640 media for 30 min at 37 °C. Cells were washed and resuspended in RPMI-1640 media supplemented with 2.5 mM Ca^{2+} and were treated with various combinations of DFMT therapies, either single target or heteroreceptor DFMT for 1 h. Then, cells were washed with PBS and taken for imaging.

2.12. Mitochondrial depolarization

JC-1 mitochondrial membrane potential sensor (Thermo Scientific) was used to evaluate the extent of mitochondrial depolarization of Raji cells. Raji cells were subjected to various single target and combination DFMT treatments for 24 h. After 24 h, cells were collected, washed, and treated with JC-1 (100 μL PBS, 4 μM) for 30 min at 37 °C. For positive depolarized control, untreated cells were treated with CCCP (0.5 μM) and incubated simultaneously with JC-1 for 30 min. After JC-1 treatment, cells were washed and resuspended in PBS for flow cytometry or confocal microscopy analysis using 488 nm excitation with 530 / 30 nm and 585 / 42 nm band-pass filters. All experiments were carried out in triplicate with multiple replicates.

2.13. Caspase 3 activation

Caspase 3 activation was evaluated using a PhiPhiLux®-G_1D_2 kit (OncoImmunin, Gaithersburg, MD) according to the manufacturer's recommended protocol. Raji cells were subjected to various combinations of single target or combination DFMT treatments for 24 h, followed by washing with PBS and caspase 3 activation analysis.

2.14. Lysosomal enlargement

Lysosome enlargement was examined by comparing lysosome size of untreated Raji cells to DFMT treated cells after 24 h. Lysosomal enlargement leads to lysosomal membrane integrity depletion resulting in reactive oxygen formation and catalytic enzymes released into the cytosol. Lysosomal enlargement of DFMT-treated Raji cells was analyzed by treating Raji cells (2×10^5) with various combinations of DFMT for 24 h, followed by treatment with LysoTracker Green DND-26 (200 nM) for 20 min at 37 °C. Fluorescence intensity of the lysosome label was quantified using flow cytometry and normalized to untreated control. Each experiment was performed in triplicate and replicated two times.

2.15. Reactive oxygen species

The presence of reactive oxygen species in the cytosol after 24 h DFMT treatments was quantified by oxidation of 2′,7′-dichlorodihy-drofluorescein diacetate (H_2DCFDA). Raji cells (2×10^5) were treated with various combinations of either single target or heteroreceptor DFMT for 24 h followed by incubation with H_2DCFDA (5 μM) for 30 min at

37 °C. Cells were washed with PBS and analyzed with flow cytometry. Each experiment was performed in triplicate and replicated two times.

2.16. Inhibition of type II apoptotic mechanisms of action with latrunculin B

Dual-target DFMT apoptosis induction, lysosomal enlargement, and homotypic cell adhesion were assayed using the actin polymerization inhibitor, Latrunculin B. Assays were performed as per above either with or without the pre-treating the Raji cells with Latrunculin B (10 μM) for 45 min at 37 °C. Latrunculin B treated cells were then washed with PBS and DFMT treatments were conducted as described above.

2.17. Translocation of heteroreceptors into lipid rafts

Observations made during the mitochondrial depolarization confocal microscopy experiments hinted at the possibility that heteroreceptor DFMT induced translocation of receptors into lipid rafts which leads to homotypic cell adhesion where lipid rafts in one cell membrane associate through various protein-protein interactions with the lipid rafts of a neighboring cell in a process known as *homotypic cell adhesion*. Heteroreceptor DFMT-treated cells observed in the mitochondrial depolarization experiments appeared to be undergoing homotypic cell adhesion, as seen by extensive “clumping” of cells that were impossible to break apart with simple pipetting. Homotypic cell adhesion was tested for by immunostaining a protein associated with lipid rafts. Raji cells (2×10^5) were treated with various combinations of single target or heteroreceptor DFMT for 6 h. Cy5-labeled Fab's were used to label location of Fab' on the cell surface. After 6 h, cells were immunostained with Alexa Fluor-555 conjugated cholera toxin B subunit (10 μg/mL) for 1 h at 4 °C. The cells were then imaged via confocal microscopy. Overlay of Cy5 fluorescence with Fluor-555 fluorescence indicated receptors translocated to lipid rafts. Homotypic cell adhesion was indicated by co-expression fluorescence at the interface of cell-cell membranes.

2.18. In vivo therapeutic efficacy

Female, 8-week-old SCID C·B-17 mice were intravenously (i.v.) injected with 4×10^6 human Non-Hodgkin Lymphoma (Raji) cells in 200 μL PBS via tail vein (Day 0). Mice were randomly distributed into treatment cohorts that included: saline, Fab'_{RTX} DFMT, Fab'_{DARA} DFMT, and Fab'_{RTX} + Fab'_{DARA} DFMT. Each DFMT treatment cohort was further divided into two groups who received either a single DFMT dose or a triple DFMT dose. Single dose treatment groups received a Fab’-MORF1 (1 nmol) i.v. injection followed by an HSA-$(MORF2)_{10}$ i.v. injection 5 h later on Day 1. Triple dose treatment groups received the same dose schedule on Days 1, 3, and 5. Mice were monitored for the onset of hind-limb paralysis and attributed weight loss as the experimental end point. Upon onset of hind-limb paralysis, mice were sacrificed, femurs removed, bone marrow collected, and bone marrow was assayed for presence of human B cells by immunostaining with *APC*-anti-human CD19 (mouse IgG1, κ isotype) and *PE*-anti-human CD10 (mouse IgG1, κ isotype).

2.19. Statistical analysis

Statistical analyses were performed using Microsoft Excel and Prism. No samples were omitted from any statistical calculations. Sample groups were compared using one-way ANOVA followed by Tukey test, $p < 0.05$ was considered statistically significant. Experiments were performed in triplicate ($n = 3$) and replicated at least two times. Percent apoptotic cells was determined by summation of quadrants one, two and four – indicating PI^+, Annexin V/PI +/+, and Annexin V^+, respectively. Magnitude of fluorescence for various cell mechanism experiments using flow cytometry were quantified using the geometric mean average function. In all cell experiments, treated cells were compared to untreated cell control groups and fluorescence is presented as "Normalized to Untreated" or "Fold Increase over Untreated", as specified. For all combination index experiments, only data points within the sigmoidal region of the titration curves were used during parameter calculations. Data points with F_a above 0.95 or below 0.05 were not used.

3. Results and discussion

3.1. Synthesis and characterization of DFMT nanoconjugates

All Fab'-based nanoconjugates were synthesized according to previously reported protocols from our group [38]. Two anti-CD20 (RTX and OBN) and two anti-CD38 (DARA and ISA) monoclonal antibodies were enzymatically digested with pepsin, then reduced with TCEP, to yield the respective Fab' fragments (Fab'_{RTX}, Fab'_{OBN}, Fab'_{DARA}, and Fab'_{ISA}) with reactive thiols. Each Fab' fragment was conjugated to a single-stranded, morpholino oligomer nucleotide (MORF1, 25 bp, 8631 g/mol, $\varepsilon = 278{,}000\ M^{-1}\ cm^{-1}$) [16]. MORF1 was conjugated to freshly synthesized Fab' through an $SM(PEG_2)$ linker to yield the desired Fab'-MORF1 "Targeting Motif" (Fig. 1A). The "Crosslink-Inducing Macromolecule", $HSA-(MORF2)_x$, was synthesized in a similar fashion utilizing reactivity of primary amines from lysine residues on the periphery of the albumin molecule. Albumin amines were reacted with $SM\text{-}PEG_2$, effectively decorating the albumin molecule with maleimide groups at the periphery ($HSA\text{-}(PEG_2\text{-Maleimide})_y$). In parallel, the 3′ disulfide-modified complementary morpholino oligonucleotide strand (MORF2, 25 bp, 8585 g/mol, $\varepsilon = 252{,}120\ M^{-1}\ cm^{-1}$) was reduced using TCEP to yield a reactive thiol at the 3′ end [16]. The freshly reduced MORF2 was conjugated through thiol-maleimide *click* chemistry yielding the desired multivalent crosslink-inducing macromolecule $HSA-(MORF2)_x$ (Fig. 1C). All Fab'-MORF1 intermediates, final nanoconjugates and the $HSA-(MORF2)_x$ were characterized by size-exclusions chromatography (Figs. 1D,E and S1), BCA assay and UV–Vis spectroscopy to determine purity, protein concentration and MORF concentration, respectively. The ratio of [MORF] to [protein] gave the MORF valency of each nanoconjugate (Fig. 1B). Hybridization of the Fab'-MORF1 nanoconjugates with $HSA-(MORF2)_x$ were confirmed by SEC and UV–Vis spectroscopy by mixing small aliquots of the two complementary molecules and observing absorbance changes at $\lambda = 260$ nm at varying molar ratios of MORF1:MORF2 (Figs. S2, S3).

3.2. DMFT nanoconjugates induce apoptosis in Raji cells both in vitro and in vivo

Raji cells, a Non-Hodgkin Lymphoma cell line positive for both CD20 and CD38, were used for all in vitro and in vivo experiments. CD20 and CD38 expression levels were estimated

by treating cells with RTX or DARA mAbs for 1 h at 4 °C, followed by PBS wash. Cells were then treated with a Fluor488 goat anti-human secondary antibody for 1 h at 4 °C in 1 *w/w%* BSA PBS solution. Level of CD20 expression was about 2-fold higher than CD38 (Fig. S4). DFMT experiments in vitro were performed over two sequential steps which models the in vivo mechanism of action. First, the Fab'-MORF1 targeting motif is added to the cells and allowed time to incubate and bind to the target receptors on the cell surface. In a time-dependent manner, the cells are collected, washed with PBS and treated with the crosslink-inducing motif. The two-step DFMT approach allows for removal of any free, unbound Fab'-MORF1 nanoconjugate from the cell suspension which would wastefully hybridize with MORF2's on the crosslink inducer. In vivo, the DFMT system is administered in a similar fashion – over two doses with a time lag between doses to allow for clearance of unbound targeting motif from the blood. Within the time lag, the off-target bound Fab'-MORF1 nanoconjugate is internalized and degraded in the lysosomes. Alternatively, the two nanoconjugate solutions can be mixed together and allow for hybridization to occur before administration [16,17,37].

3.3. Heteroreceptor DFMT increases apoptosis over single-target DFMT

To test the hypothesis that co-clustering heteroreceptors on a cell surface enhances efficacy of individual receptor clustering, we first assessed increase in efficacy in vitro by apoptosis assays using CD20+ / CD38+ Raji cells. Four Fab'-MORF1 targeting motifs – two CD20-targeting Fab's (Fab'$_{RTX}$-MORF1 and Fab'$_{OBN}$-MORF1) and two CD38-targeting Fab's (Fab'$_{DARA}$-MORF1 and Fab'$_{ISA}$-MORF1) were synthesized. Two-step DFMT protocol was followed; however, instead of a single Fab'-MORF1 treatment for the first step, a Fab'-MORF1 "cocktail" of one anti-CD20 and one anti-CD38 Fab'-MORF1 (at one-half the concentration of each) was used to target both CD20 and CD38 receptors simultaneously. Four combinations of one anti-CD20 + one anti-CD38 Fab'-MORF1 were used. Cells were incubated for 1 h, followed by a PBS wash to remove any excess or unbound Fab'-MORF1. Cells were then resuspended in fresh medium and treated with the crosslink-inducing macromolecule, HSA-(MORF2)$_{10}$ for 24 h. Our hypothesis was MORF1-MORF2 hybridization would occur indiscriminately of which Fab' the MORF1 was bound to, resulting in crosslinking of CD20 receptors with CD38 receptors on the cell surface. Efficacy was assessed in vitro by Annexin V / PI staining of co-crosslinked DFMT-treated cells compared to individual receptor DFMT-treated cells. Fab'-MORF1 combination treatments proceeded at a total [MORF1] concentration of 50 nM. Controls for individual receptor DFMT were performed at [MORF1]'s of 50 nM and 25 nM.

The dual-target DFMT system provides a platform with interchangeable targeting moieties that circumvents the need for cumber-some synthetic and purification protocols which would be needed to obtain the analogous bispecific antibody (bsAb). And although the field of bispecific antibodies has progressed toward a more high-throughput capacity, expression and purification of desired bsAbs are still required [39,40]. Dual-target DFMT provides the advantage of using pre-existing, FDA approved mAbs and simple conjugation chemistry to produce a library of Fab'-MORF1 nanoconjugates that can be paired and administered as a targeting mixture for desired antigens.

Several important findings were observed from these initial experiments that lead us to investigate concentration-dependent DFMT and to evaluate synergistic potential of heteroreceptor crosslinking. First, all four heteroreceptor DFMT combinations increased Raji cell apoptosis levels over individual DFMT-treated cells (Fig. 2A). Each individual DFMT possessed different efficiency to induce apoptosis over the same 24 h treatment period. Fab'$_{DARA}$ DFMT induced apoptosis in about 30% of the cells, Fab'$_{ISA}$ DFMT induced apoptosis in about 50%, Fab'$_{RTX}$ DFMT induced apoptosis in about 50%, and Fab'$_{OBN}$ DFMT induced apoptosis in about 70% of the cells. The differences between anti-CD20 and anti-CD38 DFMT's can be related to receptor expression, where CD20 is about two-fold higher (Fig. S4); however, the differences between Fab'$_{DARA}$ DFMT to Fab'$_{ISA}$ DFMT and Fab'$_{RTX}$ DFMT to Fab'$_{OBN}$ DFMT could be due to different binding epitopes coupled with divergent down-stream mechanisms of action inherent to the Fab'-receptor interactions [12,30,35]. The difference in efficacy between two Fab' DFMT systems targeting the same receptor prompted us to investigate synergistic versus additive versus antagonistic effects of heteroreceptor DFMT using computational methods (discussed in Section 3.5).

The second important observation was the no statistical difference between [MORF1] of 25 nM compared to 50 nM in the individual DFMT control groups. We postulate a certain threshold saturation of surface Fab'-receptor binding events will lead to a maximal apoptotic effect. Certainly not every receptor on the cell surface needs a Fab'-MORF1 bound and crosslinked to kill the cell. At 50 nM and 25 nM, we must be above this Fab'-receptor apoptotic threshold and no therapeutic efficacy improvement can be observed upon increasing the treatment concentration further. This led us to pursue DFMT titration experiments to assess concentration of Fab'-MORF1 needed to produce the desired apoptotic effect (discussed in more detail in Section 3.4 below). Finally, we wanted to prove CD20 receptors could in fact physically crosslink with CD38 receptors on the cell surface. We sought to rule out the possibility that the increased efficacy of heteroreceptor DFMT was not due to pockets of CD20 crosslinked with other CD20 molecules in one area of the cell and pockets of CD38 crosslinked with other CD38 molecules in a separate area of the cell. To prove CD20 is indeed crosslinking with CD38 within individual microdomains, we devised a FRET strategy where the CD20-targeting Fab'-MORF1 was labeled with Cy3 and the CD38-targeting Fab'-MORF1 was labeled with Cy5, Cy3-Fab'$_{RTX}$-MORF1 and Cy5-Fab'$_{DARA}$-MORF1, respectively [41,42]. Raji cells could then be treated with both fluorescently labeled Fab'-MORF1s and the emission of Cy5 when exciting with Cy3 could be quantified using flow cytometry and imaged with confocal microscopy (Fig. 2B,C). We compared the Cy5 FRET emission of cells treated with both fluorescent Fab'-MORF1 crosslinked with HSA-(MORF2)$_{10}$ to cells treated with both fluorescent Fab'-MORF1s without crosslinking. We postulated Cy5 FRET emission should increase when receptors are forced into proximity upon crosslinking. Indeed, both flow cytometry and confocal microscopy confirmed the significant increase in Cy5 emission upon Cy3 excitation between crosslinked and un-crosslinked cells. The data seem to be supported by dSTORM (direct stochastic optical reconstruction microscopy) determination of cluster size of crosslinked CD20 by Fab'$_{RTX}$-MORF1 and P-(MORF2)$_x$ (P is the *N*-(2-hydroxypropyl)methacrylamide copolymer backbone) CD20; lipid raft cluster radii are ~200 nm [43].

Other dual-target immunotherapeutic strategies (beyond bispecific antibodies constructs) are being developed in pre-clinical studies [44-48]. Yu et al. developed a dual-target platform technology based on immunoliposomes [44]. Liposomes were decorated with two different Abs targeting either CD37, CD19, or CD20, in various combinations. The authors observed a significant increase in apoptosis of malignant B cells when crosslinking heteroreceptors compared to liposomes with only a single Ab. Mi et al. demonstrated dual-target Ab nanoparticles (DINPs) induced knockdown of two immune checkpoint antagonist receptors simultaneously, leading to robust T cell activation and anti-cancer efficacy [45]. DINPs targeting PD-1 and OX40 on target cancer cells out-performed co-administration of individual single-target NPs and Ab therapies in an in vivo murine model. Passariello et al. developed aptamer-conjugated antibodies capable of either binding two antigens on the cancer cell or binding to one cancer antigen and one T cell antigen [48]. The authors demonstrated an anti-PD-L1 antibody conjugated with an epidermal growth factor receptor antagonist led to more potent cancer cell killing and more robust T cell activation than individual therapies. Finally, multivalent short chain variable fragment (scFv) chains provide a method to combine binding domains of two different scFvs in dimer, trimer or tetrameric arrangements [49-51]. These multivalent scFv molecules provide receptor clustering to induce desired cell signaling and have been investigated for treatment of disease [51]. With various dual-target immunotherapeutic systems being developed, we believe dual-target DFMT provides a unique adaption to multi-targeting systems stemming from the two-step approach of the DFMT system. Separation of the targeting motif from the therapeutic step of crosslink induction allows for easy customization of antigen combinations. Other systems rely on molar ratio conjugation steps to generate ratios of hetero Fab' conjugation, whereas our approach allows for specific concentrations of desired Fab'-MORF1 targeting moieties. The high level of customizability of Fab'-MORF1 *cocktails* allows for more cancer cell-specific DFMT therapies to be produced with ease. Systems described above require additional synthesis, purification and characterization of each new combination.

3.4. Single-target DFMT achieves single-digit nanomolar and even picomolar EC_{50}'s

To evaluate DFMT on a concentration-based assay, single-target Fab' DFMT titration experiments were conducted for all four Fab'-MORF1 nanoconjugates. Cell viability was assessed using Annexin V/PI treatments to stain for apoptotic cells. We found metabolic cell viability assays, such as CCK8, were not reliable for indicating apoptotic cells. We surmise apoptotic cells measured after 24 h of DFMT treatment could still have metabolic activity capable of cleaving small molecule metabolic assays, giving a false number of unaffected cells. Therefore, cells were subjected to two-step DFMT as described above. CD38+/CD20+ Raji cells were treated with serially diluted concentrations of Fab'-MORF1 (1 μM, 100 nM, 10 nM, 1 nM, 100 pM, and 10 pM) for 1 h followed by PBS wash. Cells were resuspended in fresh medium and treated with coinciding concentrations of HSA-$(MORF2)_{10}$ for 24 h. After 24 h, cells were collected, washed with PBS, stained with Annexin V/PI and analyzed using flow cytometry. Cells positive for Annexin V and PI in each treatment group were normalized and plotted as an EC_{50} curve (Fig. 3A). Additionally, Fab'-MORF1 binding at each concentration was assessed using fluorescently labeled Fab'-MORF1 nanoconjugates (either Cy3- or Cy5-labeled). Cells were incubated with serially diluted concentrations of labeled Fab'-MORF1 for 1 h at 4 °C in 0.5% *w*/w BSA PBS solution. Unbound Fab'-

MORF1 was removed with a PBS wash and fluorescence quantified using flow cytometry. Fluorescence was normalized and plotted against DFMT-induced apoptosis for each Fab'-MORF1 at each concentration (Fig. 3A). Plotting Fab'-MORF1 binding against Fab' DFMT-induced apoptosis allowed us to make some interesting correlations. First, the induced apoptosis from Fab' DFMT treatments remained at a maximum even when Fab'-MORF1 binding dropped off. Apoptosis induction began to decrease only after Fab'-MORF1 binding dropped down to about 10% of maximum. This suggests only about 10% of target surface receptors need a Fab'-MORF1 bound for DFMT to provide its maximal therapeutic effect. Induced apoptosis continues to decline in a sigmoidal trend with concentration. Additionally, the EC_{50} values determined by these Fab' DFMT titration experiments proved to be very low: Fab'_{DARA} DFMT = 420 ± 30 pM, Fab'_{ISA} DFMT 650 ± 150 pM, Fab'_{RTX} DFMT = 2.3 ± 0.7 nM, and Fab'_{OBN} DFMT = 1.1 ± 0.3 nM (Fig. 4D). This compares with similar dual-target immunotherapy systems which have EC_{50}'s on the order of single digit nanomolar to hundreds of picomolar [29,52].

3.5. Heteroreceptor DFMT produces synergistic apoptotic effects

A thorough Fab' DFMT combination index data set was constructed using Chou-Talalay algorithms [53] to distinguish true synergistic effects from additive effects when using anti-CD20 Fab' DFMT in combination with anti-CD38 Fab' DFMT. Chou-Talalay theory derives drug combination data from the "median-effect equation". The median-effect equation is the line fit through experimentally obtained data points of cell viability when cells are treated with a combination of two or more therapeutics. The cell viability data points in the sigmoidal region of the EC_{50} curve are plotted against the combined dose as a logarithmic function. Combination Index Plots can be plotted to evaluate synergism, antagonism or additive effects of drug combinations at various fractions of affected cells (F_a). Combination Index (CI) values define synergism as CI < 1; antagonism as CI > 1; and additive effects as CI ≅ 1. These algorithms are suitable for evaluating nanoconjugates [42].

Combination DFMT, using one anti-CD20 Fab'-MORF1 and one anti-CD38 Fab'-MORF1 simultaneously, was evaluated. A Median-Effect Plot of the four possible Fab' DFMT combinations was constructed to determine EC_{50} values (defined by the x-intercept of the linear regression) for each combination experiment [53]. The Combination Index for each data point was calculated using eq. 1:

$$CI = \frac{[Fab'MORF1]_{CD20comb.}}{[Fab'MORF1]_{CD20alone\,x}} + \frac{[Fab'MORF1]_{CD38comb.}}{[Fab'MORF1]_{CD38alone\,x}} \quad (1)$$

where $[Fab'MORF1]_{CD20alone\,x}$ = dose of anti-CD20 Fab'-MORF1 used to produce x affected cells (F_a) and $[Fab'MORF1]_{CD20comb.}$ = dose of anti-CD20 Fab'-MORF1 used in the combination experiment to produce the same F_a. CI values were calculated for each combination and plotted against F_a. CI values for ED_{75}, ED_{90}, and ED_{95} are reported in Fig. 4D. Combination Fab' DFMT Median-Effect Plots and Combination Index Plots are reported in Fig. 4. EC_{50} values for combination DFMT's (defined as the x-axis of the Median-Effect Plot) were found to be in the range of 1.3 nM to 700 pM, demonstrating the potency of the DFMT system. Importantly, CI values for all four combinations approached values <1 at higher F_a indicating true synergistic value when crosslinking CD20 with

CD38. Specific dosing information, Median-Effect Plots, Combination Index Plots and curve fit data can be found in supplemental information (Figs. S5 - S9). Fab'_{ISA} + Fab'_{RTX} combination DFMT had the lowest CI values of the four different combinations followed by Fab'_{DARA} + Fab'_{OBN} DFMT and Fab'_{ISA} + Fab'_{OBN} DFMT. Fab'_{DARA} + Fab'_{RTX} had CI values slightly below 1 in the ED_{75} – ED_{95} range.

3.6. α-CD20/α-CD38 combination DFMT induced apoptosis via Ca^{2+} influx and mitochondrial depolarization

To better understand the intracellular apoptotic mechanisms of action involved when crosslinking heteroreceptors on the cell surface, various in vitro cellular apoptotic pathways were assayed [15]. Mitochondrial viability of Raji cells after either single-target or combination DFMT was investigated first. We have previously demonstrated significant calcium influx has a key role in DFMT receptor crosslinking [21]. Here we compared calcium influx of single-target DFMT systems to the four combination DFMT systems. Raji cells were pre-treated with a calcium indicator (Fluo-3 AM, 5 μM) for 30 min at 37 °C. Cells were washed and resuspended in Ca^{2+}-infused RPMI-1640 medium (2.5 mM [Ca^{2+}]) and two-step DFMT was performed for 1 h. Then, cells were washed and resuspended in PBS buffer for Fluo-3 AM fluorescence examination by either confocal microscopy or flow cytometry (Fig. 5A). Exaggerated shifts in the Fluo-3 AM fluorescence histograms were observed with all four combinations Fab' DFMT treated Raji cells compared to single-target Fab' DFMT systems indicating a more pronounced Ca^{2+} ion influx. Free calcium in the cytosol has depolarization effects on mitochondrial membranes. The magnitude of heteroreceptor Fab' DFMT-induced mitochondrial depolarization was quantified using the polarization sensor JC-1. In healthy mitochondria, membrane polarization remains intact and JC-1 molecules aggregate in mitochondria and fluoresce red. Depolarized mitochondria allow passive diffusion of JC-1 molecules, aggregation is lost, and JC-1 monomers fluoresce green. The magnitude of green JC-1 fluorescence in DFMT-treated cells indicates the level of mitochondrial depolarization. Mitochondrial depolarization of Raji cells treated with either single-target DFMT or combination DFMT were assessed (Fig. 5B). Each Fab' DFMT combination treatment had significantly increased mitochondrial depolarization than individual Fab' DFMT therapies. Confocal microscopy images clearly show high amounts of green fluorescence compared to individual Fab' DFMT systems indicating significantly higher levels of mitochondrial depolarization. The increase in JC-1 monomer fluorescence was further confirmed and quantified using flow cytometry. Downstream effects of mitochondrial depolarization, such as caspase 3 activation (Fig. 5C), cytochrome C release and Bcl-2/Bax expression (Fig. S11) were subsequently assayed with significantly increased caspase 3 activation identified in all Fab' DFMT combination treatment groups compared to single-target Fab' DFMT groups (Fig. 5C).

3.7. α-CD20/α-CD38 combination DFMT induced Type II mAb mechanisms of action

Interestingly, the mitochondrial depolarization confocal microscopy images (Fig. 5B) suggested homotypic cell adhesion was occurring in heteroreceptor crosslinked treatment groups. Homotypic cell adhesion is a known Type II mAb mechanism of action characterized by receptor mobilization into lipid rafts and lipid raft adhesion between neighboring cancer cells [54,55]. The result of homotypic cell adhesion is clumps of

cells adhered together at their interfaces by adhesion proteins mobilized in the lipid rafts. All four combination Fab' DFMT therapies appeared to be exhibiting this phenomenon as detected by confocal microscopy. Therefore, we posited heteroreceptor crosslinking of CD20 receptors with CD38 receptors may be also invoking Type II-like mechanisms of apoptosis. Additional Type II mechanisms of action include actin rearrangement, lysosomal enlargement and leakiness, and reactive oxygen species generation. Lysosomal enlargement was assayed by LysoTracker Green fluorescence. Raji cells were treated with either single-target or combination DFMT for 24 h followed by lysosomal stain (LysoTracker Green, 200 nM) for 20 min at 37 °C. Cells were washed with PBS and resuspended for flow cytometry analysis. Fluorescence of treated cells was normalized to untreated cell control and presented as a fold increase (Fig. 6A). A significant increase in LysoTracker fluorescence was observed in three of the four combination DFMT systems. Fab'$_{DARA}$ + Fab'$_{OBN}$ DFMT combination did not significantly increase over individual therapies. We believe this is due to the Fab'$_{DARA}$ DFMT system exhibiting the lowest lysosomal enlargement and Fab'$_{OBN}$ DFMT system exhibiting the highest of all single-target DFMT systems. Combining the two did not significantly elevate lysosomal fluorescence over the already high Fab'$_{OBN}$ DFMT system. Enlarged lysosomes lead to leaky and porous membranes resulting in reactive oxygen species release into the cytosol. Cytosolic reactive oxygen species were quantified using a small molecule detector (H2DCFDA) that emits fluorescence upon oxidation. Raji cells were treated with single-target Fab' DFMT or combination DFMT systems for 24 h followed by treatment with H2DCFDA (5 μM) for 30 min at 37 °C. Cells were washed with PBS, resuspended and fluorescence quantified with flow cytometry. Fluorescence of treated cells was normalized to untreated cells (control) and presented as a fold increase (Fig. 6B). Finally, homotypic cell adhesion was confirmed using the lipid raft immunostaining reagent cholera toxin B subunit (Alexa Fluor-555, 10 μg/mL). Raji cells were treated with fluorescently labeled Fab'-MORF1 nanoconjugates (Cy3- or Cy5-) and HSA-(MORF2)x as single-target Fab' DFMT or combination DFMT for 6 h followed by immunostaining with cholera toxin B for 1 h at 4 °C. Cy3-/Cy5-Fab'-MORF1 nanoconjugate fluorescence was overlayed with cholera toxin Fluor-555 fluorescence to determine presence of Fab'-MORF1 species and lipid raft proteins at the interfaces of clumped Raji cells (Fig. 6C). Cell aggregation can be seen in all four dual-target combination DFMT therapies, as well as, in Fab'$_{OBN}$ DFMT single-target DFMT-treated cell samples. OBN is a known Type II mAb and homotypic cell adhesion is a Fc-independent and actin-dependent mechanism; therefore, Fab'$_{OBN}$ DFMT retains the ability to generate homotypic cell adhesion.

3.8. Dual-target DFMT Type II apoptotic mechanisms of action could be repressed with actin inhibition

To further validate dual-target DFMT induces Type II mechanisms of action through actin-dependent homotypic cell adhesion and lysosomal enlargement, dual-target DFMT was performed in the presence of various lysosomal pathway inhibitors [56]. Latrunculin B, inhibitor of actin polymerization and disruptor of microfilament organization, was used to assay the effects of actin rearrangement inhibition on apoptosis induction, homotypic cell adhesion and lysosomal enlargement [57]. If dual-target DFMT was inducing homotypic cell adhesion, inhibition of actin polymerization should result in decreased homotypic cell adhesion leading to decreased lysosomal enlargement and decreased apoptosis efficacy. Raji

cells were treated with dual-target DFMT combinations with or without a pre-treatment of Latrunculin B (10 μM) for 24 h. Effects of actin inhibition on apoptosis-induction were analyzed using Annexin V/PI staining (Fig. 7A). Inducedapoptosis of dual-target DFMT was significantly lowered for all four dual-target DFMT combinations and Fab'_{OBN} DFMT single-target therapy in agreement with our previous data [43]. Likewise, analysis of dual-target DFMT, with or without Latrunculin B inhibitor co-treatment, inhibited the process of homotypic cell adhesion. Microscopy analysis of dual-target DFMT cells co-treated with the actin inhibitor showed complete interruption of the homotypic cell adhesion process (Fig. 7B). Inhibition of homotypic cell adhesion led to a reduction of downstream lysosomal enlargement effects (Fig. 7C). To further validate the decrease in lysosomal enlargement observed under actin inhibition, lysosomal enlargement could also be reduced using the cysteine protease inhibitor E-64 (5 μM) [58], corroborating the results of lysosomal inhibition induced by actin inhibition (Fig. 7D, Fig. S12).

3.9. Fab'_{DARA} + Fab'_{RTX} DFMT outperforms single-target DFMT in vivo

To further investigate the therapeutic efficacy of dual-target DFMT, a human NHL xenograft mouse model experiment was conducted. Female C·B-17 SCID (C·B-*Igh-1*^{b}IcrTac-*Prkdc*^{scid}) mice were used in xenograft experiments with the human NHL Raji (CD20+/CD38+) cell transplant (Fig. 8A) [16,20]. Dual-target DFMT (α-CD20/α-CD38) was compared to single-target DFMT therapies of α-CD20 or α-CD38. Fab'_{DARA}-MORF1 nanoconjugate was used as the CD38 targeting motif and Fab'_{RTX}-MORF1 nanoconjugate was used as the CD20 targeting motif, respectively. Mice were inoculated with Raji cells (4×10^6 cells/mouse) on Day 0 by tail vein injection. Single dose therapy cohorts were compared to triple dose cohorts of each therapeutic. Single dose (1 nmol Fab'-MORF1 followed by 1 nmol HSA-$(MORF2)_{10}$ with a 5 h time lag [16]) DFMT treatments were administered on Day 1 by tail vein injection. Triple dose DFMT therapies were administered on Days 1, 3, and 5. Untreated Raji lymphoma cells in the blood stream of the mice expand and infiltrate into various organs. Eventually, infiltration into the spinal cord occurs and advanced stage disease presents with hind-limb paralysis in the mice. Hind-limb paralysis can be measured and compared between treatment groups as an objective endpoint [15,59]. Furthermore, infiltration of human Raji cells into the mouse bone marrow was assayed with anti-human pan B cell marker immunostaining (PE α-hCD10 and APC α-hCD19). Mice were monitored and weighed three times per week for 150 days. After 150 days, any surviving mice were designated as “long-term” survivors. Long-term surviving mice had their femurs removed, bone marrow collected and analyzed for any hCD10+ or hCD19+ cells (Figs. S13 - S19).

The single-dose DFMT therapy cohorts survival curves are shown in Fig. 8B. Saline control mice succumbed to hind-limb paralysis at about 3–4 weeks. Any mouse that received a DFMT therapy, either single-target or dual-target, significantly extended life expectancy over control. The dual-target DFMT system resulted in a median survival of 109 days and 3/6 long-term survivors. Conversely, the α-CD38 and α-CD20 DFMT systems had median survivals of 68 days and 81 days, respectively. Dual-target DFMT had 3/6 long-term survivors compared to 0/6 mice in the α-CD38 DFMT cohort and 2/6 mice in the α-CD20 cohort. Surviving mice were sacrificed, bone marrow collected and analyzed for human B

cells. No positive stain was observed in any long-term surviving mice (Fig. 8B). A longer extended survival was observed in the triple dose mice (Fig. 8C). The triple dose median survival of the dual-target DMFT was 142 days, whereas α-CD38 and α-CD20 DFMT systems were extended to 101 days and 103 days, respectively. The triple dose dual-target DFMT treated mice had 5/6 mice live to long-term survival compared to 1/6 and 2/6 for α-CD38 and α-CD20 DFMT systems, respectively. Bone marrow of the long-term survivors was collected and stained for human B cell markers. All mice stained negative except one α-CD38 (Fig. 8C, green box, top panel) mouse which had a slight double positive population of cells (~10%) which indicates this mouse had subclinical disease in its bone marrow after 150 days. All other mice showed no markers for human B cell infiltration into bone marrow (see Figs. S13 - S19 for enlarged flow cytometry cell populations).

4. Conclusions

Heterocrosslinking of CD20 and CD38 receptors on (CD20+/CD38+) Raji cells by DFMT (Fab'-MORF1 + HSA-$(MORF2)_x$) was compared with single-receptor crosslinking. Simultaneous crosslinking resulted in enhanced apoptosis induction both in vitro and in vivo, clearly demonstrating the advantage of simultaneous engagement of two receptors. Two FDA approved mAbs (RTX and OBN) targeting CD20 and two FDA approved mAbs targeting CD38 (DARA and ISA) were used to generate DFMT Fab'-based targeting motifs. The induced apoptotic mechanisms were examined by assays relevant to mechanisms of apoptosis induction of Type I and Type II mAbs. Robust apoptosis induction was accomplished via multiple pathways that included increased calcium influx leading to exaggerated mitochondrial depolarization, caspase 3 activation, reactive oxygen species generation, cytochrome C release, and enhanced Bax expression. Additionally, all dual-target DFMT combinations led to homotypic cell adhesion and lysosomal enlargement. Combination DFMT treatment proved to be synergistic when analyzed using the Chou-Talalay combination index method (CI < 1). Furthermore, co-clustering of CD20 with CD38 on the cell surface was analyzed by FRET experiments which relied on proximity of the two receptors upon crosslinking to emit FRET fluorescence. Upon addition the DFMT crosslink-inducing motif to fluorescently labeled Fab'-decorated cells, FRET emission increased significantly indicating crosslinking of the two heteroreceptors as they were forced into proximity. Notably, the α-CD20/α-CD38 dual-targeting DFMT system was evaluated in vivo using a disseminated human NHL xenograft mouse model to demonstrate the improved anti-cancer effect of heteroreceptor crosslinking. Nanomolar doses of nanoconjugates produced long-term survivors (150 days). One nanomolar dose on Day 1: the dual-target DMFT produced 3/6 long-term survivors and the median survival was 109 days; the single-target data were 2/6 and 81 days (α-CD20), and 0/6 and 69 days (α-CD38). For three nanomolar doses on Days 1, 3, and 5, the dual-target DMFT produced 5/6 long-term survivors and the median survival was 142 days; the single-target data were 2/6 and 103 days (α-CD20), and 1/6 and 101 days (α-CD38).

The highly multivalent nature of DFMT is well suited for multi-specific engagement of antigen. One HSA-$(MORF2)_{10}$ molecule has the potential to hybridize with up to 10 Fab'-MORF1 nanoconjugates. Based on the premise of bispecific antibody engagement, we developed an innovative new approach that attempts to crosslink two different receptors

on a target cell surface. The heteroreceptor-targeting via DFMT provides a multi-targeting platform technology capable of tailorable adaptability based on a patient's individual expression profile. The potential of such a system could lead to improved efficacy over single-target immunotherapy systems by producing better cancer targeting and potentially less drug-resistant relapse [10,60,61].

Supplementary Material

Refer to Web version on PubMed Central for supplementary material.

Acknowledgement

Research was supported by NIH grant RO1 CA246716 from the National Cancer Institute (to JK) and by Huntsman Cancer Institute ET grant 39024 (to DS/JY). We acknowledge support of funds in conjunction with grant P30 CS042014 awarded to Huntsman Cancer Institute. We thank core facilities, Preclinical Research Resource, Flow Cytometry, Confocal Fluorescence Microscopy, and Mass Spectrometry, for support.

References

[1]. Teras LR, DeSantis CE, Cerhan JR, Morton LM, Jermal A, Flowers CR, 2016 US lymphoid malignancy statistics by World Health Organization subtypes, CA Cancer J. Clin 66 (6) (2016) 443–459, 10.3322/caac.21357. [PubMed: 27618563]

[2]. Roloff GW, Drazer MW, Godley LA, Inherited susceptibility to hematopoietic malignancies in the era of precision oncology, JCO Precision Oncol. 5 (2021) 107–122, 10.1200/po.20.00387.

[3]. Wang J, Yang J, Kopeček J, Nanomedicines in B cell-targeting therapies, Acta Biomater. 137 (2022) 1–19, 10.1016/j.actbio.2021.10.024. [PubMed: 34687954]

[4]. Pich O, Cortes-Bullich A, Muiños F, Pratcorona M, Gonzalez-Perez A, Lopez-Bigas N, The evolution of hematopoietic cells under cancer therapy, Nat. Commun 12 (1) (2021) 1–11, 10.1038/s41467-021-24858-3. [PubMed: 33397941]

[5]. Cuesta-Mateos C, Alcaraz-Serna A, Somovilla-Crespo B, Muñoz-Calleja C, Monoclonal antibody therapies for hematological malignancies: not just lineage-specific targets, Front. Immunol 8 (2018) 1936, 10.3389/fimmu.2017.01936. [PubMed: 29387053]

[6]. Esfahani K, Roudaia L, Buhlaiga N, Del Rincon SV, Papneja N, Miller WH, A review of cancer immunotherapy: from the past, to the present, to the future, Curr. Oncol 27 (s2) (2020) 87–97, 10.3747/co.27.5223.

[7]. Hatano Y, Matsuoka H, Lam L, Currow DC, Side effects of corticosteroids in patients with advanced cancer: a systemic review, Support Care Cancer 26 (12) (2018) 3979–3983, 10.1007/s00520-018-4339-2. [PubMed: 29980905]

[8]. Barth MJ, Hernandez-Ilizaliturri FJ, Mavis C, Tsai PC, Gibbs JF, Deeb G, Czuczman MS, Ofatumumab demonstrates activity against rituximab-sensitive and -resistant cell lines, lymphoma xenografts and primary tumor cells from patients with B-cell lymphoma, Br. J. Haemotol 156 (4) (2012) 490–498, 10.1111/j.1365-2141.2011.08966.x.

[9]. Small GW, McLeod HL, Richards KL, Analysis of innate and acquired resistance to anti-CD20 antibodies in malignant and nonmalignant B cells, PeerJ 1 (2013), e31, 10.7717/peerj.31. [PubMed: 23638367]

[10]. Torka P, Barth M, Ferdman R, Hernandez-Ilizaliturri FJ, Mechanisms of resistance to monoclonal antibodies (mAbs) in lymphoid malignancies, Curr. Hematol. Malig. Rep 14 (5) (2019) 426–438, 10.1007/s11899-019-00542-8. [PubMed: 31559580]

[11]. Zhang J, Gu Y, Chen B, Mechanisms of drug resistance in acute myeloid leukemia, Onco.Targets Ther 12 (2019) 1937–1945, 10.2147/ott.S191621. [PubMed: 30881045]

[12]. Meyer S, Evers M, Jansen JHM, Buijs J, Broek B, Reitsma SE, Moerer P, Amini M, Kretschmer A, Ten Broeke T, den Hartog MT, Rijke M, Klein C, Valerius T, Boross P, Leusen JHW, New

insights in type I and II CD20 antibody mechanisms-of-action with a panel of novel CD20 antibodies, Br. J. Haematol 180 (6) (2018) 808–820, 10.1111/bjh.15132. [PubMed: 29468712]

[13]. Okroj M, Østergorg A, Blom AM, Effector mechanisms of anti-CD20 monoclonal antibodies in B cell malignancies, Cancer Treat. Rev 39 (6) (2013) 632–639, 10.1016/j.ctrv.2012.10.008. [PubMed: 23219151]

[14]. Aldeghaither DS, Zahavi DJ, Murray JC, Fertig EJ, Graham GT, Zhang Y-W, Connell A, Ma J, Jablonski SA, Weiner LM, A mechanism of resistance to antibody-targeting immune attack, Cancer Immunol. Res 7 (2) (2019) 230, 10.1158/2326-6066.cir-18-0266. [PubMed: 30563830]

[15]. Li L, Yang J, Wang J, Kopeček J, Drug-free macromolecular therapeutics induce apoptosis via calcium influx and mitochondrial signaling pathway, Macromol. Biosci 18 (1) (2018) 1700196, 10.1002/mabi.201700196.

[16]. Chu T-W, Zhang R, Yang J, Chao MP, Shami PJ, Kopeček J, A two-step, pre-targeted nanotherapy for CD20 crosslinking may achieve superior anti-lymphoma efficacy to rituximab, Theranostics 5 (8) (2015) 834–846, 10.7150/thno.12040. [PubMed: 26000056]

[17]. Yang J, Li L, Kopeček J, Biorecognition: a key to drug-free macromolecular therapeutics, Biomaterials 190-191 (2019) 11–23, 10.1016/j.biomaterials.2018.10.007. [PubMed: 30391799]

[18]. Kopeček J, Yang J, Polymer nanomedicines, Adv. Drug Deliv. Rev 156 (2020) 40–66, 10.1016/j.addr.2020.07.020. [PubMed: 32735811]

[19]. Rütter M, Miloševič N, David A, Say no to drugs: bioactive macromolecular therapeutics without conventional drugs, Adv. Drug Deliv. Rev 330 (2021) 1191–1207, 10.1016/j.jconrel.2020.11.026.

[20]. Li L, Yang J, Wang J, Kopeček J, Amplification of CD20 cross-linking in rituximab-resistant B-lymphoma cells enhances apoptosis induction by drug-free macromolecular therapeutics, ACS Nano 12 (4) (2018) 3658–3670, 10.1021/acsnano.8b00797. [PubMed: 29595951]

[21]. Gambles MT, Li J, Wang J, Sborov D, Yang J, Kopeček J, Crosslinking of CD38 receptors triggers apoptosis of malignant B cells, Molecules 26 (15) (2021) 4658, 10.3390/molecules26154658. [PubMed: 34361811]

[22]. Li L, Yang J, Soodvilai S, Wang J, Opanasopit P, Kopeček J, Drug-free albumin-triggered sensitization of cancer cells to anticancer drugs, J. Control. Release 293 (2019) 84–93, 10.1016/j.jconrel.2018.11.015. [PubMed: 30465822]

[23]. Wang J, Li L, Yang J, Clair PM, Glenn MJ, Stephens DM, Radford DC, Kosak KM, Deininger MW, Shami PJ, Kopeček J, Drug-Free Macromolecular Therapeutics induce apoptosis in cells isolated from patients with B cell malignancies with enhanced apoptosis induction by pretreatment with gemcitabine, Nanomedicine: NBM 16 (2019) 217–225, 10.1016/j.nano.2018.12.011.

[24]. Li L, Wang J, Li Y, Radford DC, Yang J, Kopeček J, Broadening and enhancing functions of antibodies by self-assembling multimerization at cell surface, ACS Nano 13 (10) (2019) 11422–11432, 10.1021/acsnano.9b04868. [PubMed: 31553883]

[25]. Saul JM, Annapragada AV, Bellamkonda RV, A dual-ligand approach for enhancing targeting selectivity of therapeutic nanocarriers, J. Control. Release 114 (2006) 277–287, 10.1016/j.jconrel.2006.05.028. [PubMed: 16904220]

[26]. Yu B, Mao Y, Yuan Y, Yue C, Wang X, Mo X, Jarjoura D, Paulaitis ME, Lee RJ, Byrd JC, Lee LJ, Muthusamy N, Targeted drug delivery and cross-linking induced apoptosis with anti-CD37 based dual-ligand immunoliposomes in B chronic lymphocytic leukemia cells, Biomaterials 34 (2013) 6185–6193, 10.1016/j.biomaterials.2013.04.063. [PubMed: 23726226]

[27]. Blanco B, Domínguez-Alonso C, Alvarez-Vallina L, Bispecific immunomodulatory antibodies for cancer immunotherapy, Clin. Cancer Res 27 (20) (2021) 5457, 10.1158/1078-0432.CCR-20-3770. [PubMed: 34108185]

[28]. Zhou S, Liu M, Ren F, Meng X, Yu J, The landscape of bispecific T cell-engager in cancer treatment, Biomark. Res 9 (1) (2021) 38, 10.1186/S40364-021-00294-9. [PubMed: 34039409]

[29]. Oostindie SC, van der Horst HJ, Kil LP, Strumane K, Overdijk MB, van den Brink EN, van den Brakel JHN, Rademaker HJ, van Kessel B, van den Noort J, Chamuleau MED, Mutis T, Lindorfer MA, Taylor RP, Schuurman J, Parren PWHI, Beurskens FJ, Breij ECW, DuoHexaBody-CD37®, a novel biparatopic CD37 antibody with enhanced Fc-mediated

hexamerization as a potential therapy for B-cell malignancies, Blood Cancer J. 10 (3) (2020) 30, 10.1038/S41408-020-0292-7. [PubMed: 32341336]

[30]. Awasthi A, Ayello J, van de Ven C, Elmacken M, Sabulski A, Barth MJ, Czuczman MS, Islam H, Klein C, Cairo MS, Obinutuzumab (GA101) compared to rituximab significantly enhances cell death and antibody-dependent cytotoxicity and improves overall survival against CD20(+) rituximab-sensitive/−resistant Burkitt lymphoma (BL) and precursor B-acute lymphoblastic leukaemia (pre-BALL): potential targeted therapy in patients with poor risk CD20(+) BL and pre-BALL, Br. J. Haematol 171 (5) (2015) 763–775, 10.1111/bjh.13764. [PubMed: 26471982]

[31]. Cavallini C, Galasso M, Pozza ED, Chignola R, Lovato O, Dando I, Romanelli MG, Krampera M, Pizzolo G, Donadelli M, Scupoli MT, Effects of CD20 antibodies and kinase inhibitors on B-cell receptor signalling and survival of chronic lymphocytic leukaemia cells, Br. J. Haematol 192 (2) (2021) 333–342, 10.1111/bjh.17139. [PubMed: 33216963]

[32]. Pavlasová G, Mráz M, The regulation and function of CD20: an “enigma” of B-cell biology and targeted therapy, Hematologica 105 (6) (2020) 1494–1506, 10.3324/haematol.2019.243543.

[33]. Overdijk MB, Jansen JHM, Nederland M, Lammerts van Bueren JJ, Groen RWJ, Parren PWHI, Leusen JHW, Boross P, The therapeutic CD38 monoclonal antibody daratumumab induces programmed cell death via Fcγ receptor-mediated crosslinking, J. Immunol 197 (2016) 807–813, 10.4049/jimmunol.1501351. [PubMed: 27316683]

[34]. Liao S, Liang L, Yue C, He J, He Z, Jin X, Luo G, Zhou Y, CD38 is involved in cell energy metabolism via activating the PI3K/AKT/mTOR signaling pathway in cervical cancer cells, Int. J. Oncol 57 (1) (2020) 338–354, 10.3892/ijo.2020.5040. [PubMed: 32319590]

[35]. Richter J, Sanchez L, Thibaud S, Therapeutic potential of isatuximab in the treatment of multiple myeloma: evidence to date, Semin. Oncol 47 (2–3) (2020) 155–164, 10.1053/j.seminoncol.2020.04.004. [PubMed: 32446599]

[36]. Chou T-C, Drug combination studies and their synergy quantification using the Chou-Talalay method, Cancer Res. 70 (2) (2010) 440–446, 10.1158/0008-5472.Can-09-1947. [PubMed: 20068163]

[37]. Zhang L, Fang Y, Yang J, Kopeček J, Drug-free macromolecular therapeutics: impact of structure on induction of apoptosis in Raji B cells, J. Control. Release 263 (2017) 139–150, 10.1016/j.jconrel.2016.12.025. [PubMed: 28024916]

[38]. Zhang L, Fang Y, Li L, Yang J, Radford DC, Kopeček J, Human serum albumin-based drug-free macromolecular therapeutics: apoptosis induction by coiled-coil-mediated cross-linking of CD20 antigens on lymphoma B cell surface, Macromol. Biosci 18 (11) (2018), e1800224, 10.1002/mabi.201800224. [PubMed: 30259654]

[39]. Hofmann T, Krah S, Sellmann C, Zielonka S, Doerner A, Greatest hits – innovative technologies for high throughput identification of bispecific antibodies, Int. J. Mol. Sci 21 (18) (2020) 6551, 10.3390/ijms21186551.

[40]. Labrijn AF, Janmaat ML, Reichert JM, Parren PWHI, Bispecific antibodies: a mechanistic review of the pipeline, Nat. Rev. Drug Discov 18 (8) (2019) 585–608, 10.1038/s41573-019-0028-1. [PubMed: 31175342]

[41]. Hatterer E, Barba L, Noraz N, Daubeuf B, Aubry-Lachainaye J-P, von der Weid B, Richard F, Kosco-Vilbois M, Ferlin W, Shang L, Buatois V, Co-engaging CD47 and CD19 with a bispecific antibody abrogates B-cell receptor/CD19 association leading to impaired B-cell proliferation, mAbs 11 (2) (2019) 322–334, 10.1080/19420862.2018.1558698. [PubMed: 30569825]

[42]. Meyer BH, Martinez KL, Segura J-M, Pascoal P, Hovius R, George N,Johnsson K, Vogel H, Covalent labeling of cell-surface proteins for in-vivo FRET studies, FEBS Lett. 580 (6) (2006) 1654–1658, 10.1016/j.febslet.2006.02.007. [PubMed: 16497304]

[43]. Hartley JM, Chu T-W, Peterson EM, Zhang R, Yang J, Harris J, Kopeček J, Super-resolution imaging and quantitative analysis of membrane protein/lipid raft clustering mediated by cell surface self-assembly of hybrid nanoconjugates, ChemBioChem 16 (2015) 1725–1729, 10.1002/cbic.201500278. [PubMed: 26097072]

[44]. Yu B, Mao Y, Yuan Y, Yue C, Wang X, Mo X, Jarjoura D, Paulaitis ME, Lee RJ, Byrd JC, Lee LJ, Muthusamay N, Targeted drug delivery and cross-linking induced apoptosis with anti-CD37 based dual-ligand immunoliposomes in B chronic lymphocytic leukemia cells, Biomaterials 34 (26) (2013) 6185–6193, 10.1016/j.biomaterials.2013.04.063. [PubMed: 23726226]

[45]. Mi Y, Smith CC, Yang F, Qi Y, Roche KC, Serody JS, Vincent BG, Wang AZ, A dual immunotherapy nanoparticle improves T-cell activation and cancer immunotherapy, Adv. Mater 30 (25) (2018) 1706098, 10.1002/adma.201706098.

[46]. Li J, Lin W, Chen H, Xu Z, Ye Y, Chen M, Dual-target IL-12-containing nanoparticles enhance T cell functions for cancer immunotherapy, Cell. Immunol 349 (2020), 104042, 10.1016/j.cellimm.2020.104042. [PubMed: 32061376]

[47]. Niwa T, Kasuya Y, Suzuki Y, Ichikawa K, Yoshida H, Kurimoto A, Tanaka K, Morita K, Novel immunoliposome technology for enhancing the activity of the agonistic antibody against the tumor necrosis factor receptor superfamily, Mol. Pharm 15 (9) (2018) 3729–3740, 10.1021/acs.molpharmaceut.7b01167. [PubMed: 29648839]

[48]. Passariello M, Camorani S, Vetrei C, Cerchia L, De Lorenzo C, Novel human bispecific aptamer-antibody conjugates for efficient cancer cell killing, Cancers 11 (9) (2019), 10.3390/cancers11091268.

[49]. Monnier PP, Vigouroux RJ, Tassew NG, In vivo applications of single chain Fv (variable domain) (scFv) fragments, Antibodies 2 (2) (2013) 193–208, 10.3390/antib2020193.

[50]. Wittel UA, Jain M, Goel A, Chauthan SC, Colcher D, Batra SK, The in vivo characteristics of genetically engineered divalent and tetravalent single-chain antibody constructs, Nucl. Med. Biol 32 (2) (2005) 157–164, 10.1016/j.nucmedbio.2004.11.003. [PubMed: 15721761]

[51]. Cuesta ÁM, Sainz-Pastor N, Bonet J, Oliva B, Álvarez-Vallina L, Multivalent antibodies: when design surpasses evolution, Trends Biotechnol. 28 (7) (2010) 355–362, 10.1016/j.tibtech.2010.03.007. [PubMed: 20447706]

[52]. Gupta P, Goldenber DM, Rossi EA, Cardillo TM, Byrd JC, Muthusamy N, Furman RR, Chang C-H, Dual-targeting immunotherapy of lymphoma: potent cytotoxicity of anti-CD20/74 bispecific antibodies in mantle cell and other lymphomas, Blood 119 (16) (2012) 3767–3778, 10.1182/blood-2011-09-381988. [PubMed: 22271448]

[53]. Chou T-C, Clinical studies of combination chemotherapy for cancer, in: Rideout DC (Ed.), Synergism and Antagonism in Chemotherapy, Clinical Studies of Combination Chemotherapy for Cancer, Academic Press, Inc, 1991, pp. 103–108.

[54]. Yu J, Song Y, Tian W, How to select IgG subclasses in developing anti-tumor therapeutic antibodies, J. Hematol. Oncol 13 (1) (2020) 45, 10.1186/S13045-020-00876-4. [PubMed: 32370812]

[55]. Owen CJ, Stewart DA, Obinutuzumab for the treatment of patients with previously untreated chronic lymphocytic leukemia: overview and perspective, Ther. Adv. Hematol 6 (4) (2015) 161–170, 10.1177/2040620715586528. [PubMed: 26288711]

[56]. Morton WM, Ayscough KR, McLaughlin PJ, Latrunculin alters the actin-monomer subunit interface to prevent polymerization, Nat. Cell Biol 2 (6) (2000) 376–378, 10.1038/35014075. [PubMed: 10854330]

[57]. Alduaij W, Ivanov A, Honeychurch J, Cheadle EJ, Potluri S, Lim SH, Shimada K, Chan CHT, Tutt A, Beers SA, Glennie MJ, Cragg MS, Illidge TM, Novel type II anti-CD20 monoclonal antibody (GA101) evokes homotypic adhesion and actin-dependent, lysosome-mediated cell death in B-cell malignancies, Blood 117 (17) (2011) 4519–4529, 10.1182/blood-2010-07-296913. [PubMed: 21378274]

[58]. Šubr V, Duncan R, Hanada K, Cable HC, Kopeček J, A lysosomotropic polymeric inhibitor of cysteine proteinases, J. Control. Release 4 (1986) 63–68, 10.1016/0168-3659(86)90034-9.

[59]. Chu T-W, Yang J, Zhang R, Sima M, Kopeček J, Cell surface self-assembly of hybrid nanoconjugates via oligonucleotide hybridization induces apoptosis, ACS Nano 8 (1) (2014) 719–730, 10.1021/nn4053827. [PubMed: 24308267]

[60]. Gottesman MM, Mechanisms of cancer drug resistance, Annu. Rev. Med 53 (1) (2002) 615–627, 10.1146/annurev.med.53.082901.103929. [PubMed: 11818492]

[61]. Hall MD, Handley MD, Gottesman MM, Is resistance useless? Multidrug resistance and collateral sensitivity, Trends Pharmacol. Sci 30 (10) (2009) 546–556, 10.1016/j.tips.2009.07.003. [PubMed: 19762091]

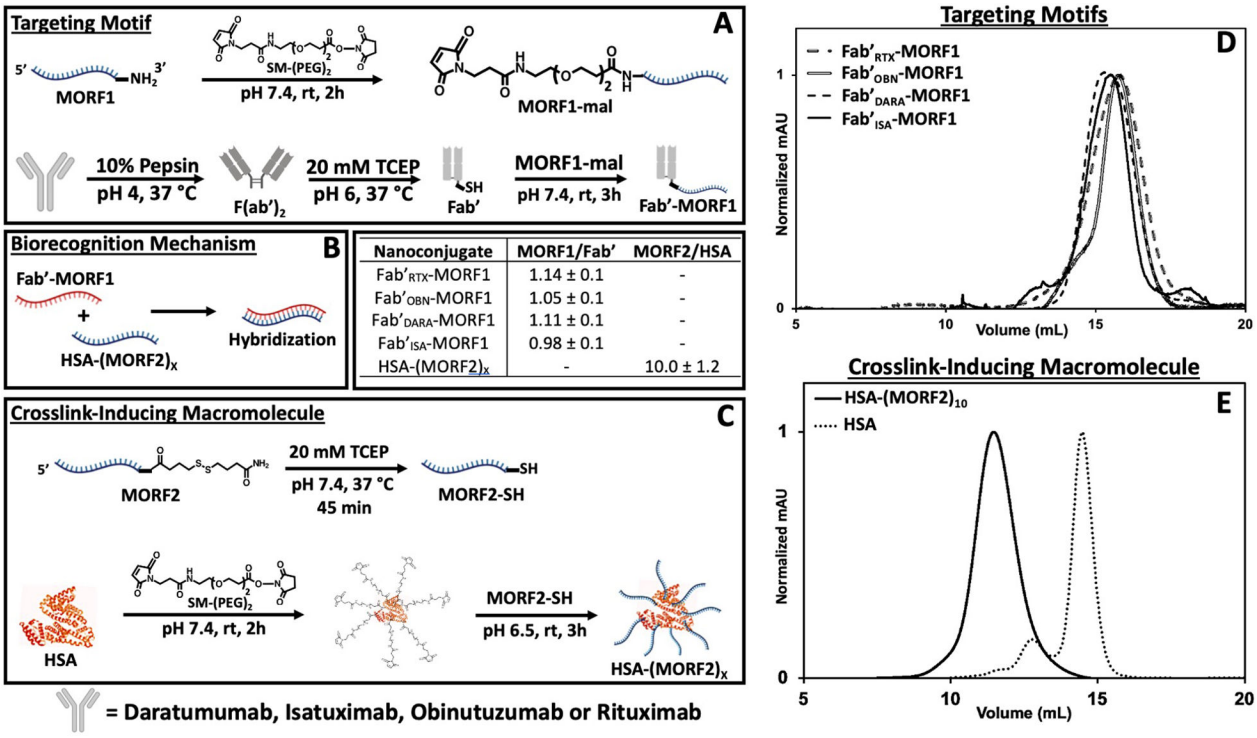

Fig. 1.

Nanoconjugate synthesis and characterization. **(A)** Synthetic route to generate Fab'-MORF1 nanoconjugates. Whole antibody represents either DARA, ISA, OBN, or RTX. All nanoconjugates contain diethyleneglycol as the spacer inserted by SM-PEG_2. **(B)** Valency characterization of nanoconjugates as determined by BCA assay and UV–Vis to determine the ratio of MORF concentration to protein concentration. **(C)** Synthetic route to generate HSA-$(MORF2)_x$. **(D)** Fab'-MORF1 nanoconjugate size exclusion chromatography profiles detected on a Superdex 200 10/300 GL column, PBS (pH 7.4) as eluant at 0.4 mL/min flow rate. **(E)** HSA-$(MORF2)_x$ nanoconjugate size exclusion chromatography profile compared to pure HSA starting material (same method as D).

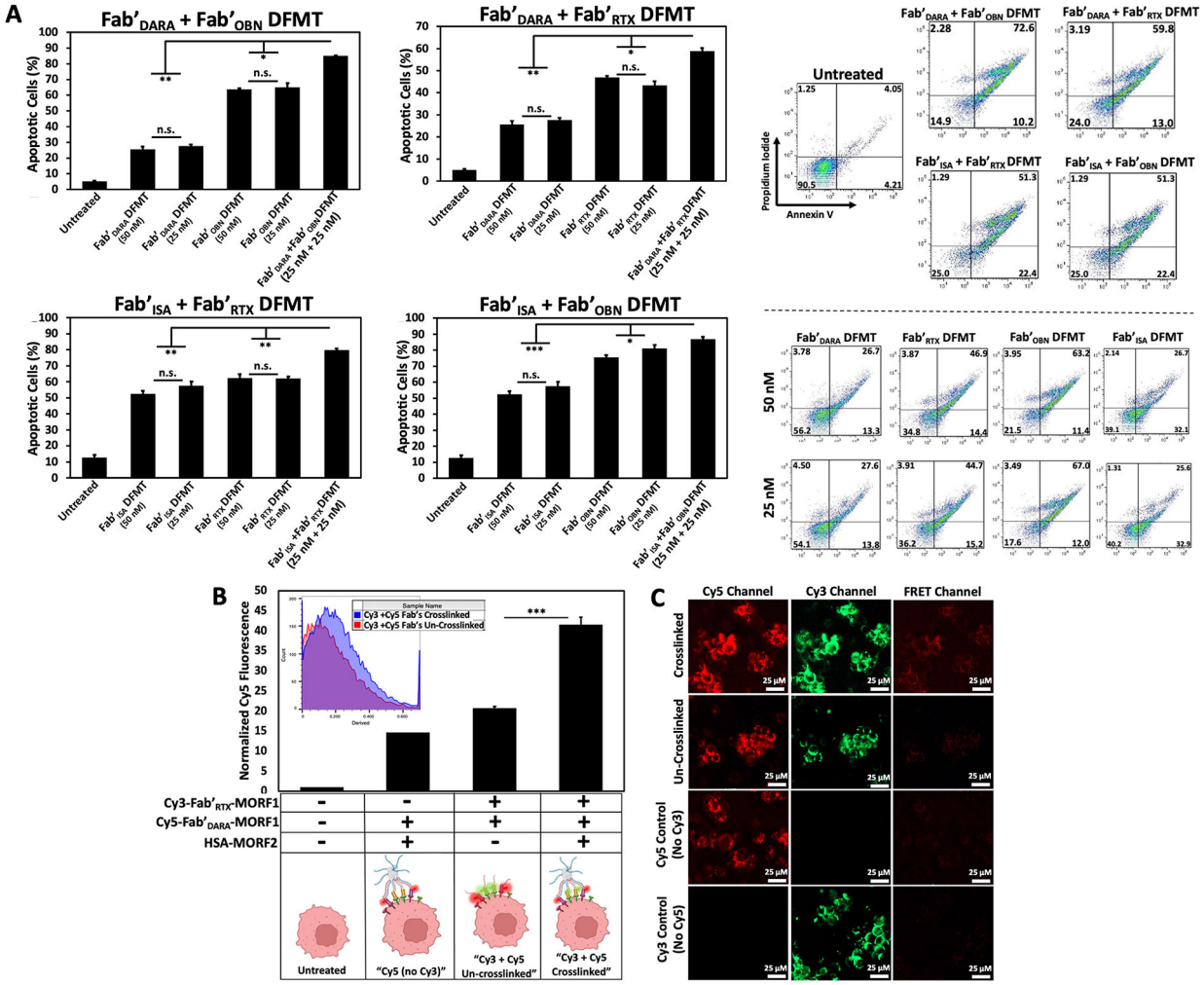

Fig. 2.

(A) Heteroreceptor DFMT-induced apoptosis on CD20+ / CD38+ Raji cells. Cell viability was measured by Annexin V and Propidium Iodide staining and analyzed by flow cytometry. Flow cytometry cell population distribution for all four heteroreceptor combinations are shown, along with representative cell population distributions for individual DFMT treatments at [MORF1] = 25 nM and 50 nM. **(B)** Flow cytometry output of FRET-induced excitation of Cy5-Fab'$_{DARA}$-MORF1 upon excitation of Cy3-Fab'$_{RTX}$-MORF1 on the cell surface. FRET emission was quantified as the amount of fluorescence observed when exciting cells with a 488 nm excitation with 530 / 30 nm band-pass filter and detecting emission 670 / 30 nm. **(C)** Confocal microscopy images of Cy3-Fab'$_{RTX}$-MORF1 and Cy5-Fab'$_{DARA}$-MORF1 treated Raji cells with or without crosslink-inducing macromolecule treatment. FRET-induced emission of Cy5 can be observed in the crosslinked treatment group, but no emission detectable in the un-crosslinked treatment group. Unlabeled Fab'$_{RTX}$-MORF1 was used for "No Cy3" control and unlabeled Fab'$_{DARA}$-MORF1 was used for "No Cy5" control. Both controls were crosslinked. All experiments were performed in triplicate. *** $p < 0.001$, ** $p < 0.01$, *$p < 0.05$, n.s. not significant by One-Way ANOVA and Tukey test.

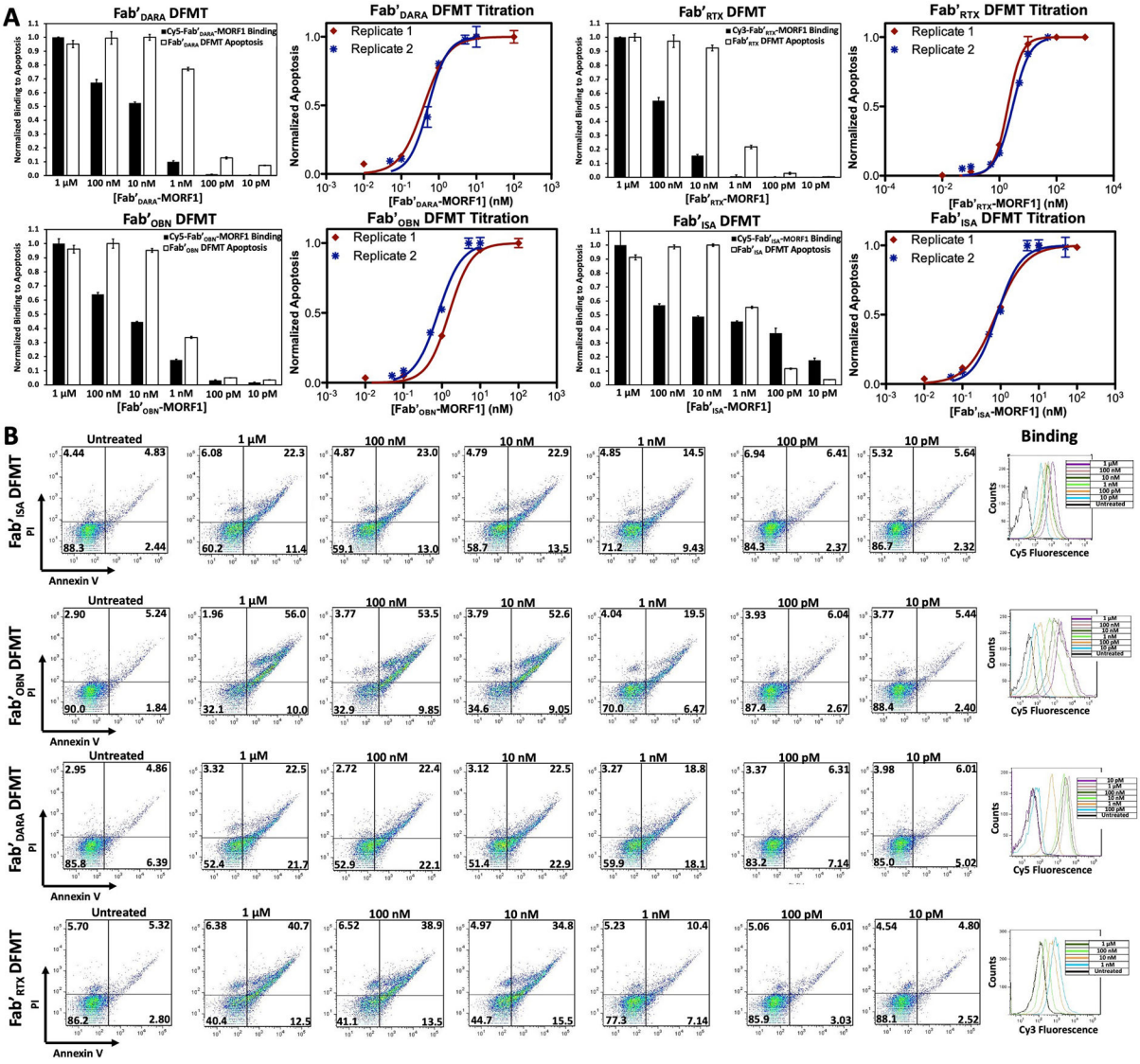

Fig. 3.

Fab' DFMT titration experiments using Annexin V / Propidium Iodide staining to identify respective EC_{50} concentrations for single-target DFMT systems. **(A)** Fab' DFMT-induced apoptosis data normalized to Fab'-MORF1 binding for each Fab' DFMT system. CD20+/CD38+ Raji cells were treated with two-step DFMT for 24 h, followed by Annexin V/PI stain and flow cytometry analysis. Separately, Raji cells were treated with fluorescently labeled Fab'-MORF1 nanoconjugates at serial dilutions. Fluorescence was quantified using flow cytometry and normalized to maximum fluorescence. Fab' DFMT-induced apoptosis and Fab'-MORF1 binding at each concentration was then overlayed. Experiments were performed in triplicate and in two replicates. EC_{50} concentrations for each Fab' DFMT system was determined using a logarithmic EC_{50} curve fit function in Prism. **(B)** Flow cytometry cell population distribution data for the apoptosis experiments and the labeled Fab'-MORF1 fluorescence histograms.

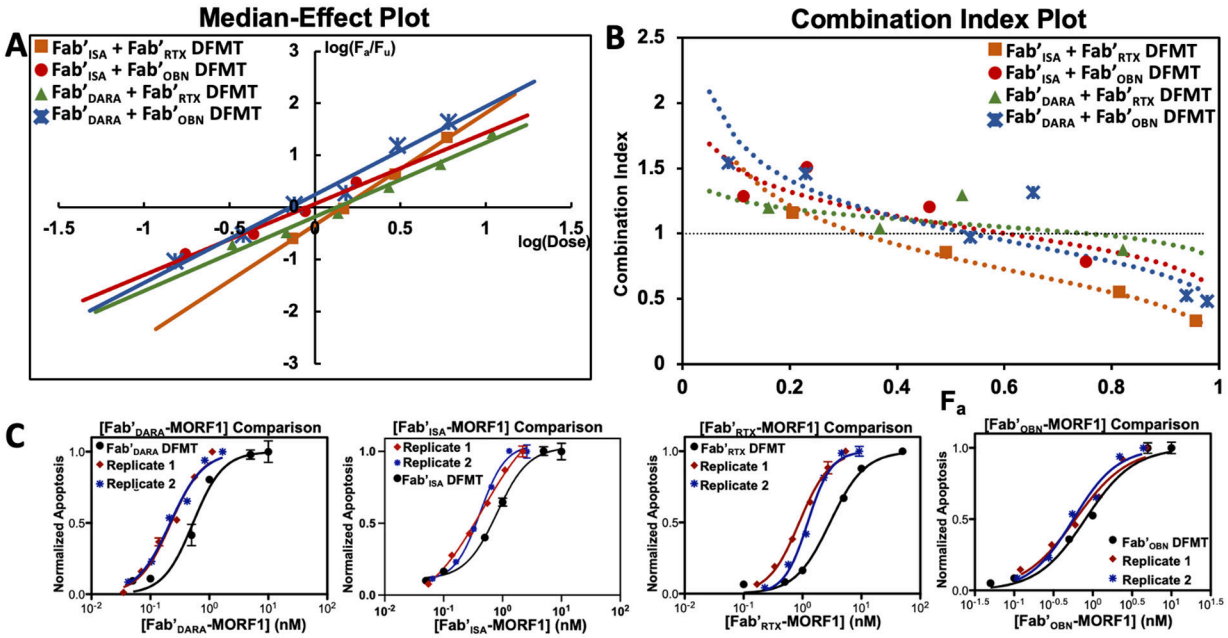

D

Treatment	EC_{50} (nM)	CI at ED_{75}	CI at ED_{90}	CI at ED_{95}
Fab'_{DARA} DFMT	0.420 ± 0.030	-	-	-
Fab'_{ISA} DFMT	0.650 ± 0.150	-	-	-
Fab'_{RTX} DFMT	2.3 ± 0.70	-	-	-
Fab'_{OBN} DFMT	1.1 ± 0.30	-	-	-
Fab'_{DARA} + Fab'_{RTX} DFMT	1.3 ± 0.090	0.95 ± 0.07	0.94 ± 0.02	0.93 ± 0.07
Fab'_{DARA} + Fab'_{OBN} DFMT	0.700 ± 0.030	0.77 ± 0.08	0.69 ± 0.02	0.65 ± 0.07
Fab'_{ISA} + Fab'_{RTX} DFMT	1.3 ± 0.2	0.68 ± 0.12	0.55 ± 0.15	0.47 ± 0.16
Fab'_{ISA} + Fab'_{OBN} DFMT	0.94 ± 0.07	0.97 ± 0.10	0.89 ± 0.17	0.84 ± 0.21

Fig. 4.

Anti-CD20 / anti-CD38 combinational Fab' DFMT experiments analyzed using Chou-Talalay combination index method. **(A)** Median-Effect Plot overlay of the four Fab' DFMT combination cell viability experiments. Data points collected in the sigmoidal region of the combination EC_{50} plots were plotted as $\log(F_a/F_u)$ on the y-axis and log(combined Fab'-MORF1 dose) on the x-axis. Linear regression was used to get a line fit of the data. The x-intercept of the regression curve was taken as the EC_{50} concentration. **(B)** Combination Index Plot overlay of the four Fab' DFMT combination cell viability experiments. Data points from the Median-Effect Plot were converted to Combination Index values using Eq. 1 and plotted against F_a. Combination Index values at 75% Effective Dose, 90% Effective Dose, and 95% Effective Dose are reported and found to be <1, indicating synergism. **(C)** Representative EC_{50} plots overlayed with individual Fab' DFMT and combination Fab' DFMT with dose of identified Fab'-MORF1 on the x-axis. **(D)** Tabulated EC_{50} values for individual Fab' DFMT systems and combination Fab' DFMT systems in nanomolar. Combination Index values at ED_{75}, ED_{90}, and ED_{95} are reported for each of the four Fab' DFMT combination systems. All experiments were performed in triplicate and in two replicates. The average and standard deviation of the two replicates is reported.

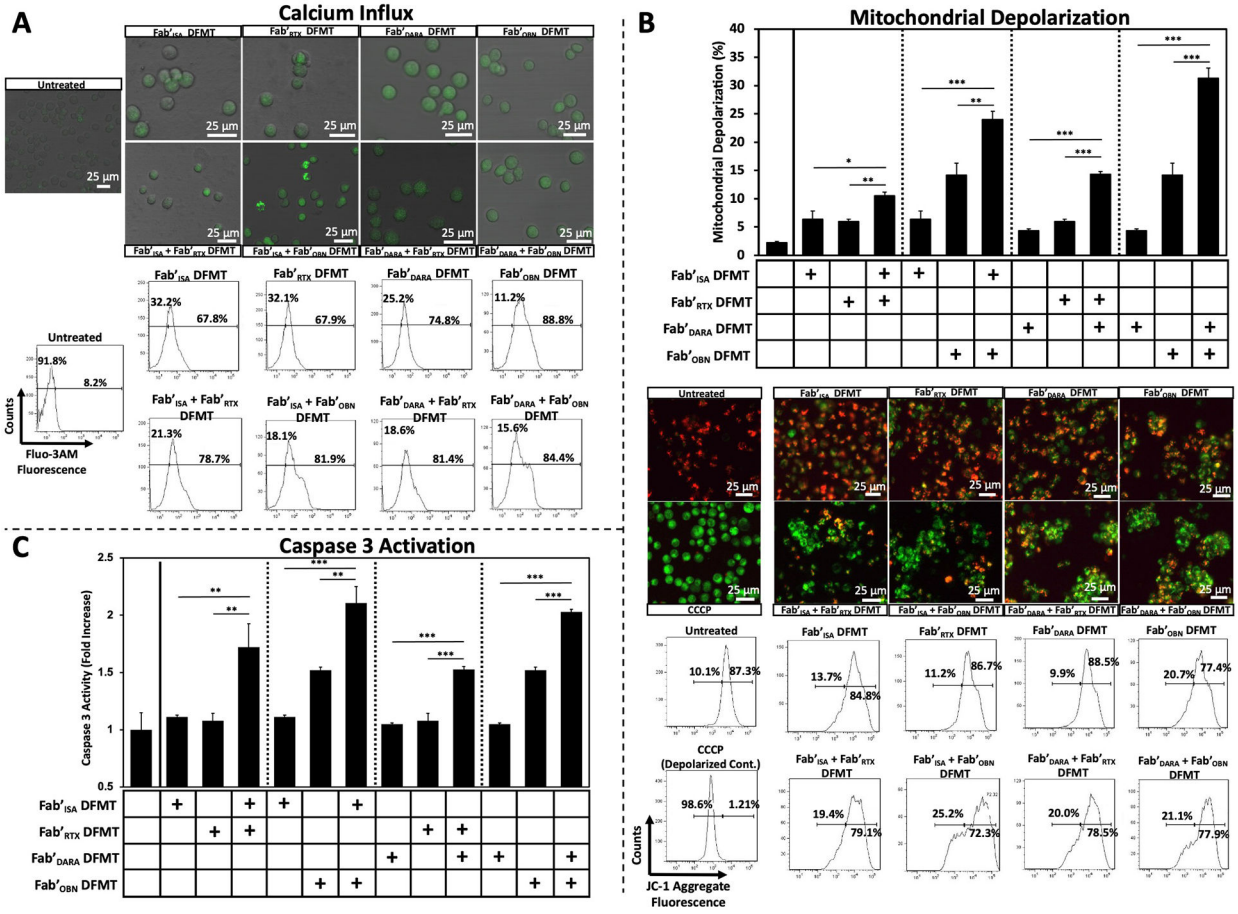

Fig. 5.

Various Type I monoclonal antibody apoptosis mechanisms of action assays for Raji cells treated with single-target Fab' DFMT systems and heteroreceptor DFMT systems. **(A)** Calcium influx quantification of single-target DFMT systems compared to heteroreceptor DFMT systems *(Top of Panel A)*. Confocal microscopy images of Raji cells preloaded with calcium indicator Fluo-3 AM indicator. Cells were treated with various DFMT systems for 1 h, washed and imaged to compare qualitative fluorescence intensities *(Bottom of Panel A)*. Flow cytometry histograms of Fluo-3 AM fluorescence of Raji cells treated with the indicated DFMT systems. Untreated cells were gated for background fluorescence. Histogram shifts from untreated were recorded. **(B)** Mitochondrial membrane depolarization quantification using JC-1 red/green fluorescence. Fluorescence intensities of Raji cells treated with various Fab' DFMT treatments were quantified with flow cytometry (upper bar graph and lower histogram data) and imaged using confocal microscopy (middle of panel B). Positive membrane depolarization control was performed by treated cells with CCCP to depolarize mitochondrial membranes completely. Homotypic cell adhesion is visible in heterocrosslinked images. **(C)** Caspase 3 activity of Raji cells treated with various Fab' DFMT therapies was assayed using a PhiPhiLux® kit and quantified using flow cytometry. Flow cytometry histograms of Caspase 3 experiments can be found in Fig. S10. All experiments were performed in triplicate. *** $p < 0.001$, ** $p < 0.01$, * $p < 0.05$, n.s. not significant by One-Way ANOVA and Tukey test.

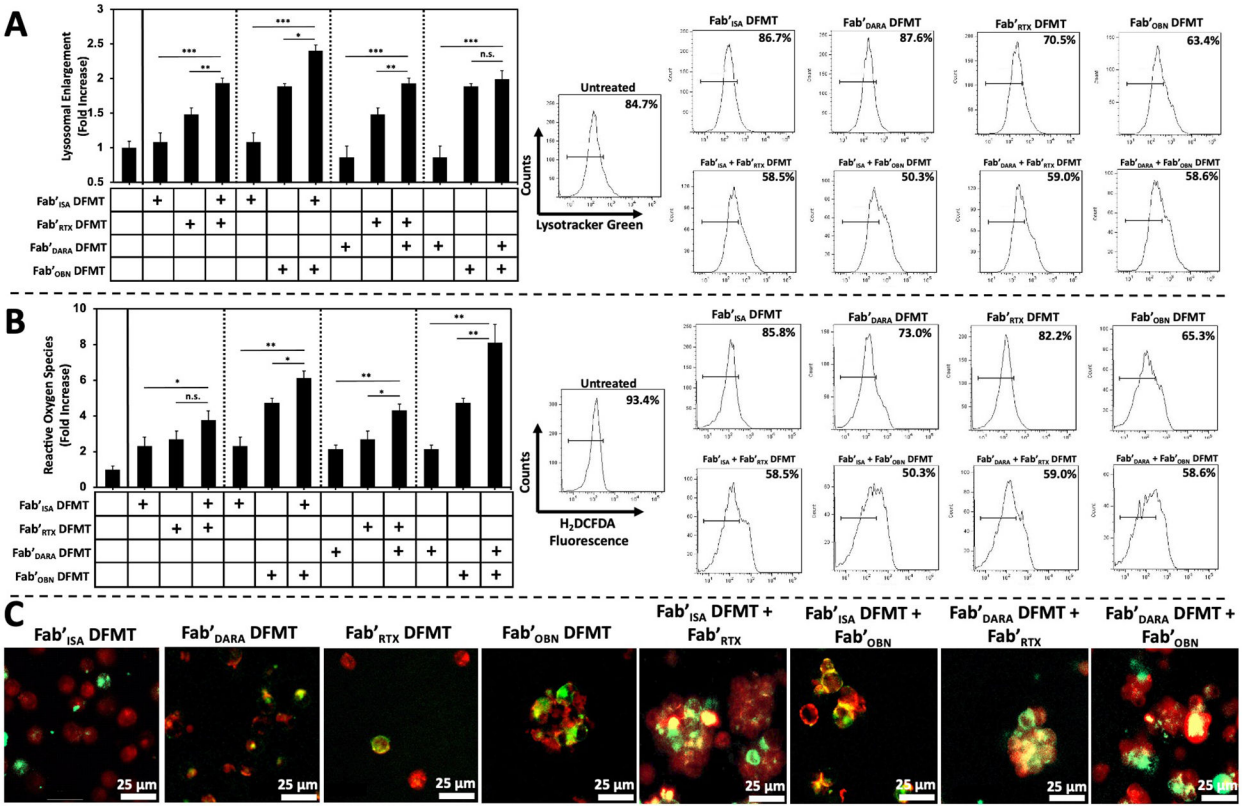

Fig. 6.

Type II mAb mechanism of action assays. **(A)** Lysosomal enlargement flow cytometry quantification using LysoTracker Green fluorescence to measure degree of lysosomal involvement in Raji cells treated with single-target DFMT systems compared to combination DFMT systems. Bar graph represents LysoTracker Green fluorescence intensity normalized to untreated cell control. The histograms represent the fluorescence shift increase from untreated control cells. **(B)** Reactive oxygen species flow cytometry quantification using H_2DCFDA oxidation detector in Raji cells treated with single-target DFMT systems compared to combination DFMT systems. Bar graph represents H_2DCFDA fluorescence intensity normalized to untreated cell control. The histograms represent the fluorescence shift increase from untreated control cells. **(C)** Confocal microscopy images of DFMT-treated Raji cells assaying for homotypic cell adhesion comparing single-target Fab' DFMT to combination Fab' DFMT systems. DFMT-treated Raji cells were immunostained with Fluor-555 cholera toxin B subunit to label lipid raft aggregation at the interface of aggregated cells. Fluorescently labeled Fab'-MORF1 nanoconjugates were used to confirm presence of receptor-bound Fab'-MORF1 molecules at the interface of aggregated cells (yellow colour indicates overlap of Fab'-MORF1 and lipid raft marker). All experiments were performed in triplicate. *** $p < 0.001$, ** $p < 0.01$, *$p < 0.05$, n.s. not significant by One-Way ANOVA and Tukey test.

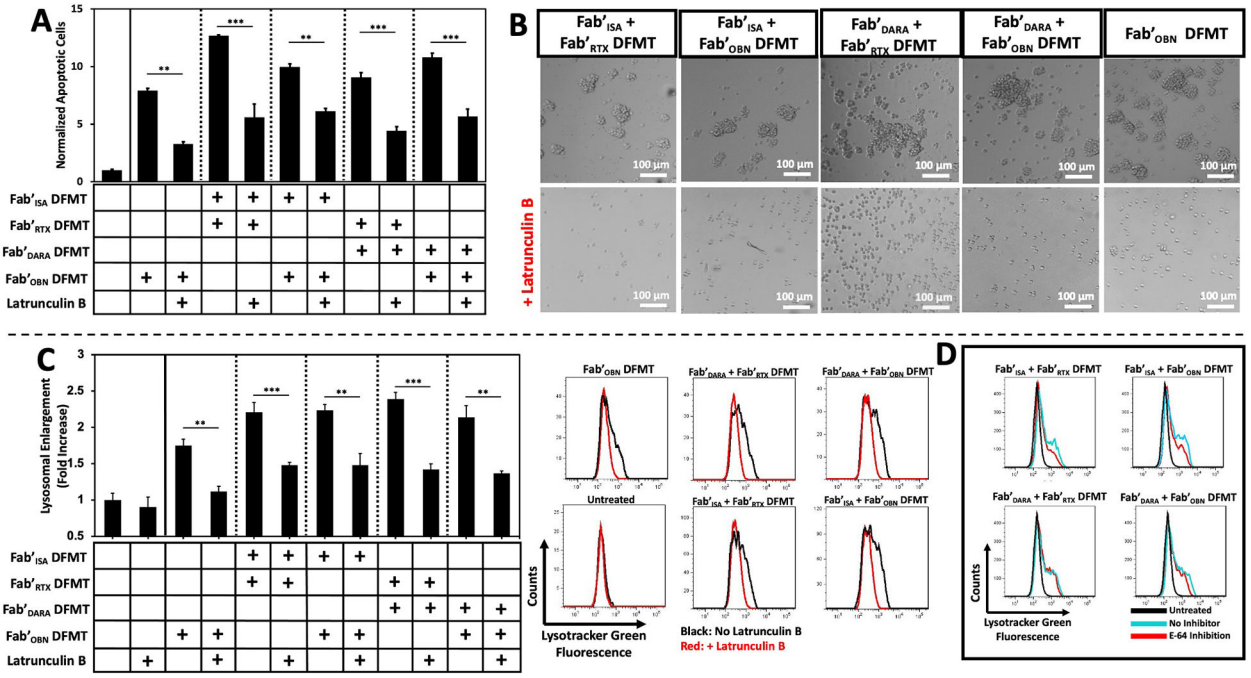

Fig. 7.

Inhibition of Type II mAb mechanisms of action. **(A)** Inhibition of dual-target DFMT apoptosis using an actin polymerization inhibitor (Latrunculin B). Raji cells were treated with combinations of dual-target DFMT with or without a pre-treatment of actin inhibitor (10 μM) for 24 h. Induced apoptosis was quantified using Annexin V/PI stain and flow cytometry. Geometric mean fluorescence of Annexin V+/PI+ cells are presented as a normalization to untreated control cells. **(B)** Inhibition of homotypic cell adhesion by co-treatment of Raji cells with dual-target DFMT with or without actin inhibitor (10 μM for 6 h at 37 °C). Bright field microscopy images depict Raji cells treated with dual-target DFMT (top) and cells treated with dual-target DFMT + Latrunculin B (bottom). Loss of homotypic cell adhesion (actin-dependent process) was observed. **(C)** Inhibition of lysosomal enlargement of dual-target DFMT pre-treated with or without actin inhibitor (10 μM for 24 h at 37 °C). Raji cells were subjected to 24 h dual-target DFMT therapy with or without Latrunculin B pretreatment and lysosomal enlargement was analyzed by LysoTracker Green geometric mean fluorescence quantified using flow cytometry. Bar graph represents mean fluorescence normalized to untreated control with accompanying fluorescence histograms. **(D)** Inhibition of lysosomal enlargement using the cysteine protease inhibitor, E-64. Raji cells were subjected to dual-target DFMT with or without pre-treatment of E-64 (5 μM for 24 h at 37 °C). After 24 h, cells were treated with LysoTracker Green and fluorescence was analyzed using flow cytometry. Fluorescence histograms of untreated control (black) are overlayed with dual-target DFMT (blue) and dual-target DFMT + inhibitor (red). All experiments were performed in duplicate. *** $p < 0.001$, ** $p < 0.01$ by One-Way ANOVA and Tukey test.

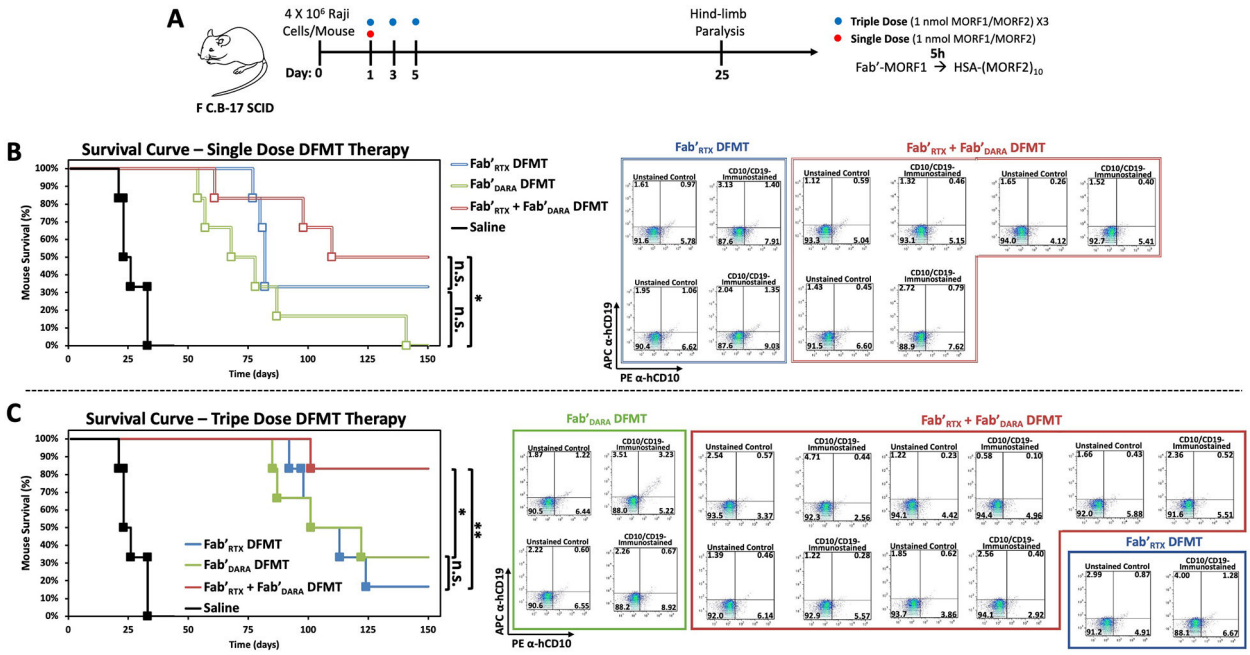

Fig. 8.

In vivo validation of dual-target DFMT efficacy on xenograft Non-Hodgkin Lymphoma in mouse. **(A)** Schematic representation of inoculation and dosing schedule. **(B)** Paralysis-free survival of single-dose DFMT-treated mice. Saline control mice (black) are compared with Fab'$_{DARA}$ DFMT-treated mice (green), Fab'$_{RTX}$ DFMT-treated mice (blue), and Fab'$_{DARA}$ + Fab'$_{RTX}$ combination DFMT-treated mice (red). Long-term surviving mice hind femur bone marrow analysis for presence of Raji (CD10+/CD19+) infiltration. Bone marrow was immunostained for hCD10 (PE α-hCD10) and hCD19 (APC α-hCD19) and analyzed by flow cytometry. **(C)** Paralysis-free survival of triple-dose DFMT-treated mice with accompanying long-term surviving mice bone marrow analysis. Cohorts consisted of six randomly distributed mice per group ($\alpha = 0.05$, power = 0.80). $^{**}p < 0.01$, $^{*}p < 0.05$, n.s. not significant by logrank (Mantel-Cox) test.